New Model-Free Daily Inversion of NOx Emissions using TROPOMI (MCMFE-NOx): Deducing a See-Saw of Halved Well Regulated Sources and Doubled New Sources

Qin Kai[1], Shi Jincheng[1], He Qin[1], Deng Weizhi[2], Wang Shuo[3], Liu Jian[4], and Cohen Jason Blake[1]

[1]China University of Mining and Technology
[2]The University of Iowa
[3]Chengdu University of Information Technology
[4]Sun Yat-Sen University

November 16, 2022

Abstract

Current approaches to estimate NOx emissions fail to account for new and small sources, biomass burning, and sources which change rapidly in time, generally don't account for measurement error, and are either based on models, or do not consider wind, chemistry, and dynamical effects. This work introduces a new, model-free analytical environment that assimilates daily TROPOMI NO2 measurements in a mass-conserving manner, to invert daily NOx emissions. This is applied over a rapidly developing and energy-consuming region of Northwest China, specifically chosen due to substantial economic and population changes, new environmental policies, large use of coal, and access to independent emissions measurements for validation, making this region representative of many rapidly developing regions found across the Global South. This technique computes a net NOx emissions gain of 70% distributed in a seesaw manner: a more than doubling of emissions in cleaner regions, chemical plants, and regions thought to be emissions-free, combined with a more than halving of emissions in city centers and at well-regulated steel and powerplants. The results allow attribution of sources, with major contributing factors computed to be increased combustion temperature, atmospheric transport, and in-situ chemical processing. It is hoped that these findings will drive a new look at emissions estimation and how it is related to remotely sensed measurements and associated uncertainties, especially applied to rapidly developing regions. This is especially important for understanding the loadings and impacts of short-lived climate forcers, and provides a bridge between remotely sensed data, measurement error, and models, while allowing for further improvement of identification of new, small, and rapidly changing sources.

New Model-Free Daily Inversion of NO_x Emissions using TROPOMI (MCMFE-NO_x): Deducing a See-Saw of Halved Well Regulated Sources and Doubled New Sources

Kai Qin[1+], Jincheng Shi[1], He Qin[1], Weizhi Deng[2,3], Shuo Wang[4], Jian Liu[2], Jason B. Cohen[1*+]

[1]Jiangsu Key Laboratory of Coal-Based Greenhouse Gas Control and Utilization, School of Environment and Spatial Informatics, China University of Mining and Technology, Xuzhou

[2]Department of Atmospheric Sciences, Sun Yat-Sen University, Zhuhai

[3]Now at: Department of Chemical & Biochemical Engineering, The University of Iowa, Iowa City, IA, USA

[4]College of Meteorological Observation, Chengdu University of Information Technology, Chengdu

[*]Correspondence to jasonbc@alum.mit.edu / jasonbc@cumt.edu.cn

+These authors contributed equally to this work

Abstract

Current approaches to estimate NO_x emissions fail to account for new and small sources, biomass burning, and sources which change rapidly in time, generally don't account for measurement error, and are either based on models, or do not consider wind, chemistry, and dynamical effects. This work introduces a new, model-free analytical environment that assimilates daily TROPOMI NO_2measurements in a mass-conserving manner, to invert daily NO_x emissions. This is applied over a rapidly developing and energy-consuming region of Northwest China, specifically chosen due to substantial economic and population changes, new environmental policies, large use of coal, and access to independent emissions measurements for validation, making this region representative of many rapidly developing regions found across the Global South. This technique computes a net NO_x emissions gain of 70% distributed in a see-saw manner: a more than doubling of emissions in cleaner regions, chemical plants, and regions thought to be emissions-free, combined with a more than halving of emissions in city centers and at well-regulated steel and powerplants. The results allow attribution of sources, with major contributing factors computed to be increased combustion temperature, atmospheric transport, and in-situ chemical processing. It is hoped that these findings will drive a new look at emissions estimation and how it is related to remotely sensed measurements and associated uncertainties, especially applied to rapidly developing regions. This is especially important for understanding the loadings and impacts of short-lived climate forcers, and provides a bridge between remotely sensed data, measurement error, and models, while allowing for further improvement of identification of new, small, and rapidly changing sources.

1. Introduction – Background

Oxides of Nitrogen (NO_x) are associated with high temperature combustion in the atmosphere, and are directly produced by fossil fuel combustion, fires, biomass burning, industry, shipping, electric discharge, and other sources (Brewer et al., 1973; Logan 1983). NO_x is one of the set of short-lived trace gasses which are considered short-lived climate forcers (SLCFs), with direct impacts on: human health, nitrate aerosol (an important component of scattering aerosols) and tropospheric ozone (which is both air pollutant and greenhouse gas) (Chen et al., 2007; Collins et al., 2013; Crutzen, 1970; Jacob et al., 1996; Li et al., 2018; Monks et al., 2015; Rollins et al., 2012; Sand et al., 2016; Seinfeld, 1989; Shindell et al., 2012; Tan et al., 2018). Presently, there are techniques to observe the local surface concentration of NO_x and the remotely sensed total column of NO_2 from both surface and satellite platforms. However, due to rapid chemical reactivity, non-linear interactions with UV radiation and VOCs, sensitivity to combustion temperature, and rapid chemical change between NO_2 and NO, there is no simple way to approximate emissions of NO_x at high spatial and temporal resolution (Alvarado et al., 2010; Lueue et al, 2001; Martin et al., 2003; Martin et al., 2006; Mijling et al., 2013).

Present methods to approximate SLCF emissions lead to results which tend to underestimate actual emissions in those regions of the world which are rapidly developing (Cohen and Wang, 2014; Lei et al., 2014; Lin et al., 2020; Wang et al., 2021). The first general method is based on sets of equations referred to as bottom-up aggregation, in which small geographic and temporal scale measurements made in the laboratory or field are aggregated together with economic and technological data (Li et al., 2017; Oliver et al., 1994; van Amstel et al., 1999). The second approach uses directly measured point-source measurements such as those made via local flux towers (Geddes and Murphy, 2014; Haszpra et al., 2018; Karl et al., 2017; Lee et al., 2015). The third approach uses chemical transport models and either a Bayesian, 3D/4D variance, or Kalman Filter type of inversion (Cohen and Wang, 2014; Henderson et al., 2012; Hu et al., 2022; Napelenok et al., 2008). A final approach is limited to special situations where there is a single very strong, non-time varying source surrounded by relatively clean upwind regions, coupled with Gaussian plume modeling (Beirle et al., 2011; Beirle et al., 2019; Cohen and Prinn, 2011; de Foy et al., 2014; Jin et al., 2021; Laughner and Cohen, 2019), or by taking the data over a long period of time during a specific season of the year and approximating a general emissions estimation, and assuming it is uniform over the averaged spatial and/or temporal domain (Kong et al., 2022). Due to the approximations associated with each method, there are some constant

problems: underapproximation or complete miss of small and moderate sources (Drysdale et al., 2022); underestimation of sources with a large amount of temporal and spatial variability (Cohen, 2014; Stavrakou et al., 2016; Vaughan et al., 2016; Wang et al., 2010; Zyrichidou et al., 2015); and over-dependence on a priori estimates (Zhao and Wang, 2009). Furthermore, other than the computationally expensive Kalman Filter approach, these methods do not provide robust uncertainly analysis (Cohen and Wang, 2014; Lin et al., 2020; Wang et al., 2021a). At the present time, emissions used to drive the loading and distribution of both aerosols and ozone in climate models rely heavily on static bottom-up approaches (Oliver et al., 1994; van Amstel et al., 1999). This has limited nearly all perturbation studies of SLCF to merely scaling up and down existing distributions in space and time to attempt to look for a scaled perturbation signal, and then averaging the resulting signal, effectively ignoring significant variations in space and time, such as wildfires and new urbanization, which are both expected to increase in magnitude in the future as the climate continues to change (Deng et al., 2021; Evangeliou et al., 2018; Lund et al., 2020).

This work introduces a new approach to compute NO_xemissions, using a mass conserving model free approximation [MCMFE-NO_x] based on daily remotely sensed column measurements of NO_2 from TROPOMI at $0.05^o \times 0.05^o$ spatial resolution, reanalysis 3-hourly wind fields, and a 4-term mass conservation approximation. This technique permits a robust quantification of the underlying thermodynamics driving the ratio of the primary emissions NO_x to NO_2, both advective and pressure-induced dynamical transport, and a first order approximation of the underlying in-situ chemical loss of NO_x. The computed uncertainty associated with each individual underlying factor as well as the remotely sensed measurements is quantified. The resulting fits allow a rapid check to determine if the underlying driving terms are consistent with known physical, chemical, and thermodynamic principles, allowing for climate-induced feedbacks on emissions to be integrated into climate runs. Since no complex modeling is required, MCMFE-NO_x is readily accessible to use in connection with the current batch of climate models, without added additional computational costs (Cohen and Prinn, 2011; Cohen et al., 2011; Holmes et al., 2013; Prinn, 2013).

MCMFE-NO_x is applied using one year of daily TROPOMI NO_2 observations over the newly developing, energy-rich, triangular-shaped region of Northwestern China called the "Golden Energy Triangle" (Chen et al., 2010; Liang et al., 2019; Ling et al., 2017; Shen et al., 2016), consisting of Ningxia, and parts of Shaanxi, Inner Mongolia, and Shanxi Provinces. This region is a large producer and consumer of coal for local power generation, export of power to commercial and highly developed regions in Eastern China (such as Jiangsu and Shanghai), steel, chemicals, materials, heavy industries, and energy-intensive desert agriculture, among other uses (Chen et al., 2010). This region consists of well-established chemical factories and urban areas in Yinchuan and Yulin, power production in Wuhai, and steel mills and urbanization in Baotou, in addition to new and rapidly expanding urban areas (Huhehaote and Eerdousi), coal-fired power production (around Wuhai), steel production (around Baotou), and chemical industry (Xiaoyi and expansion around both Yinchuan and Yulin). Due to its rapidly growing economy and large population change, there is expected to be a significant change in emissions over the last decade (Stavrakou et al., 2008; Streets and Waldhoff, 2000) as demonstrated in a set of recently taken photographs of the coal-fired power plants and chemistry plants in Ningdong and steel factories in Baotou (Figure 1). This area is well representative of the types of new industry and economic growth occurring throughout the Global South, and any biases found in the emissions from this region are likely to also be found in other rapidly developing and energy intensive regions around the world (Rogelj et al., 2014).

It is essential that emissions used to drive global and regional climate models are consistent with actual emissions to the atmosphere at high temporal and spatial resolution in order to simulate the impacts of short-lived climate forcers (Aamaas et al., 2017; Zheng and Unger, 2021). The results presented here are successful at capturing existing and growing urban areas, coal-fired power plants, chemical plants, iron and steel production, and other industrial sources, while further providing insight into what controls these sources. The impacts of changes in urban, industrial, and transportation sources associated with a growing middle class are observed, with the results comparing excellently with an independent set of measurements of small to medium industrial sources, especially so at over geographic areas in which there is no a priori emissions estimate, indicating the growing importance of moderate and small emissions sources (van der A et al.,

2020; Wang et al., 2012). Furthermore, the variability in the emissions estimates demonstrate clear impacts of meteorology, photochemistry, emissions thermodynamics, and terrain induced effects on NO_x emissions (Lin et al., 2021; Stavrakou et al., 2013; Tong et al., 2022). MCMFE-NO_x allows a consistent analysis of the natural and anthropogenic sources and in-situ evolution of NO_x emissions, and provides maps of when, where, and how to target emission controls in close-to real time. These are necessary steps for creating the next generation of emissions products which can be used to better understand the impacts of changes in the emissions of short-lived climate forcers, as well as to help better manage mitigation efforts to address these sources.

Figure 1: Recent photographs taken at Ningdong demonstrating a power plant and chemicals plant (top left), and Baotao demonstrating a steel plant (top right). A map of the region in this work, including all cities mentioned in the paper is given below.

2. Methods

2.1 Experimental Design

A graphical overview of the steps used in this work is provided in Figure 2. First, the VCDs from TROPOMI are quality controlled. Next, on a grid-by-grid, and day-by-day basis, the subset of pixels which contain valid VCDs are used in connection with a gold-standard a priori emissions database to make a monthly mass-conserving fit. These fitted values are then applied to all data, day-by-day and grid-by-grid where there is sufficient TROPOMI data, to produce emissions. In those grids which do not have best fit coefficients, a bootstrap approach is used.

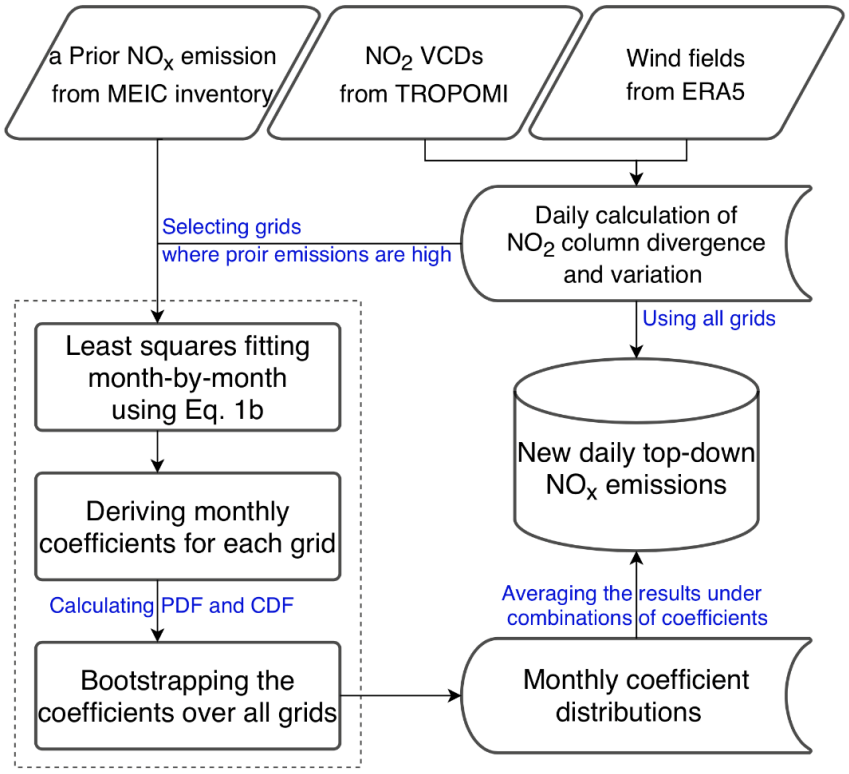

Figure 2. Flowchart describing the steps used to first develop MCMFE-NO_x.

2.2 Remotely Sensed Data

The TROPOMI spectrometer (Van Geffen et al., 2020; Veefkind et al., 2012) onboard Sentinel-5 Precursor (2017–today) has a local equator crossing time around 13:30 providing global afternoon coverage. TROPOMI measures backscattered solar UV, allowing the retrieval of the tropospheric NO_2 Vertical Column Densities (VCDs) with spatial resolution of 3.5kmx7km (3.5kmx5.5km since August 2019) at nadir. This work uses KNMI offline version 1.2/1.3 from 1 January 2019 to 31 December 2019, and further filters pixels with a qa_value <0.75. The overlapping NO_2 VCDs pixels in each swath are resampled to the common latitude-longitude grids with a size of 0.05°x0.05° using the weighted polygon shaped remotely sensed measurement toolkit HARP (http://stcorp.github.io/harp/doc/html/index.html).

There are natural factors which make this region an ideal case study for this new emissions estimation approach. The region has low cloud coverage, allowing for a higher density of remotely sensed TROPOMI measurements and higher measurement precision due to a lower level of cloud contamination (Liu et al., 2020; Platz et al., 1998). The vast majority of significant NO_x sources are separated by relatively empty land, and are of a size that they can be captured within a few grids, allowing for less complexity in terms of background effects and separation of upwind versus local sources (Cohen and Prinn, 2011). Furthermore, the climate, elevation and overall surface UV flux are somewhat similar throughout the region, indicating that chemical decay on average does not change too much.

Given the uncertainty of the NO_2 measurements is approximately $1.0\text{x}10^{15}$+30% molecules/cm^2 (computed as $1.4\text{x}10^{15}$molecules/cm^2) therefore it is important to filter any data in which the annual mean of the data is smaller than this value, so as to not estimate emissions in regions in which the only basis is potential noise (Zhang and Schreifels, 2011). Furthermore, since at most points there is a considerable amount of missing data, to be certain that the data is reliable on a month-to-month basis, the mean value when taken over all

days of the month (including missing data points) must also have a mean larger than $1.4x10^{15}$molecules/cm^2. In all cases, these values are set to NaN and subsequently are not computed further.

2.3 Emissions a priori

The Multi-resolution Emission Inventory for China (MEIC) model provides a high-resolution bottom-up emission inventory of anthropogenic air pollutants over mainland China. NO_x emissions are provided on a total monthly basis across five sectors: agriculture, industry, power, residential and transportation. This work uses emissions from MEIC at a spatial resolution of 0.1°x0.1° and a temporal resolution of monthly, corresponding to 2015, as the a prior for the mass-conserving model employed herein, which is the latest emissions inventory available China-wide. To be consistent with the other units, the monthly NO_x emissions are assumed constant day-to-day and therefore are converted to ug/$m^{-2}s^{-1}$, and this value is used as the a prior for each month. This resulting output is interpolated to the TROPOMI spatial resolution by the nearest neighbor method. For this study, we discarded the bottom 2.5 percentile of emissions, so as to ensure that the values used are not within the error range of the TROPOMI measurements. Furthermore, to ensure representativeness between the a priori data the results, especially due to the increased UV radiation and hence chemical reactivity at height, since there is no a priori emissions data available at elevations greater than 1500m, all data above this height are also set to NaN and subsequently are not computed further.

2.4 China EPA Powerplant Emissions Data

The continuous emissions monitoring system (CEMS) was introduced by the ministry of environmental protection of China (MEP) in 2007 to monitor and manage the emissions of state-controlled key coal-fired power plants and large industrial boilers (Tang et al., 2020). CEMS is designed to provide direct, real-time, continuous measurements of pollutant concentrations and air flow through the stack into the atmosphere, from coal-fired power plants, steel plants, cement plants, boilers and so on (Karplus et al., 2018; Tang et al., 2020). Each CEMS is required to provide real-time data feeds to the automatic monitoring and control system in national, provincial and municipal environmental protection agencies (Tang et al., 2020). The CEMS data used in this work was collected from the Energy Big Data network, and provides monthly data for 2017 and 2019 (http://energy.ckcest.cn/index).

2.5 Statistical Methods

Daily data from TROPOMI and the ECMWF reanalysis is grouped month-by-month at each 0.05°x0.05° spatial-grid together with the best-of-class monthly a priori emissions dataset for China using MEIC to compute the best fitting value for α_1, α_2, and α_3 grid-by-grid, month-by-month using a multiple least squares regression (MLR) fitting approach. To compute both the best 4computed, data is required both on the day of interest itself, as well as the day before, the day after, and each of the adjacent 4 grids on the day being analyzed. The horizontal gradients are specifically computed in both the x and y directions using data from four adjacent boxes on the same day as the measurement. The temporal gradients are computed using both the value from the past day, the present day, and the future day on the same grid as being computed. In terms of fitting the values of α_1, α_2, and α_3, best fits were made using MLR month-by-month and pixel-by-pixel. This approach is valid when there are at least 4 data points available for each fit of the three respective terms. For pixels in specific months that do not have enough data to make a successful fit, or a p value larger than 0.05, the values of α_1, α_2, and α_3 are set to nan.

By solving the terms month-to-month, the resulting approximations are more able to reproduce the different chemical and transport forcings observed during different times of the year. Monthly aggregated PDFs for each of α_1, α_2, and $\alpha_3$are provided respectively as figures S1-ii, S2-ii, and S3-ii at https://www.doi.org/10.6084/m9.figshare.19560517 where ii is the month, while the climatological mean values of α_1, α_2, and α_3 are given in Figure 3. There is a moderate amount of variation observed between the resulting PDFs in different months, with the largest differences observed between August (most variable distributions of α_1, α_2, and α_3) and January (least variable distributions of α_1, α_2, and α_3).

Since some of the MLR fits may occasionally lead to extreme values of α_1, α_2, and α_3 which are not physically

realistic, it is essential to find a reasonable range of coefficients to use to predict the emissions. To this aim, a bootstrap approach is used to estimate the maximum probability density of the three coefficients on a month-by-month basis. The bootstrap was done using a sampling frequency of 3000, and a confidence level of 95%. The corresponding coefficient confidence interval was obtained and compared against reasonable limits imposed by both the underlying chemistry and physics. All non-realistic terms (such as positive chemical decay rates, unreasonably fast or slow for chemistry, and ratios of NO_x/NO2 which are too small to exist in the real atmosphere) were set to nan. Furthermore, these conditions were not observed to exist in any of the post bootstrap outputs.

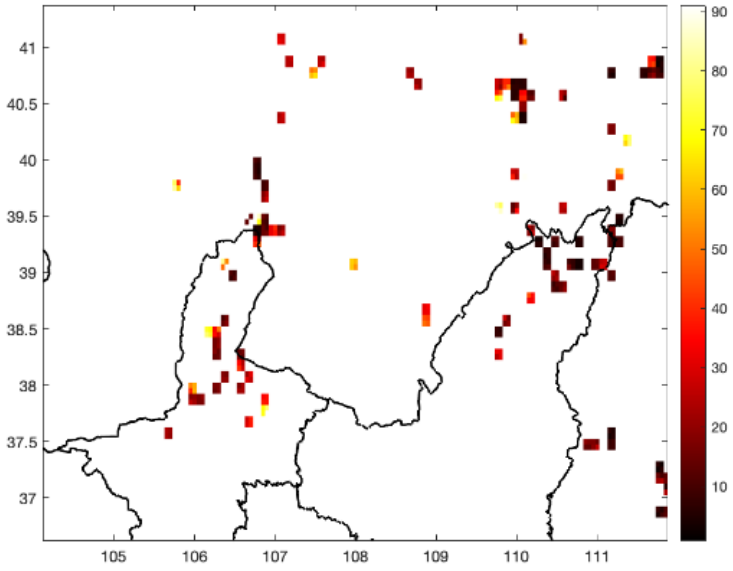

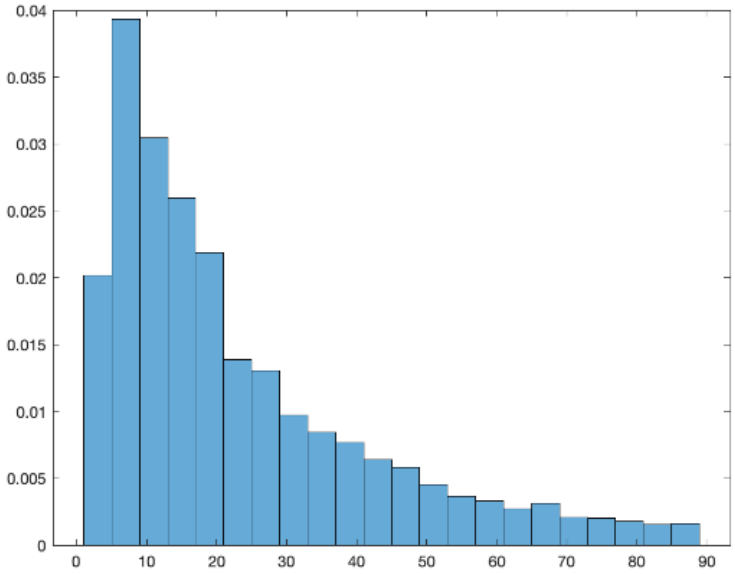

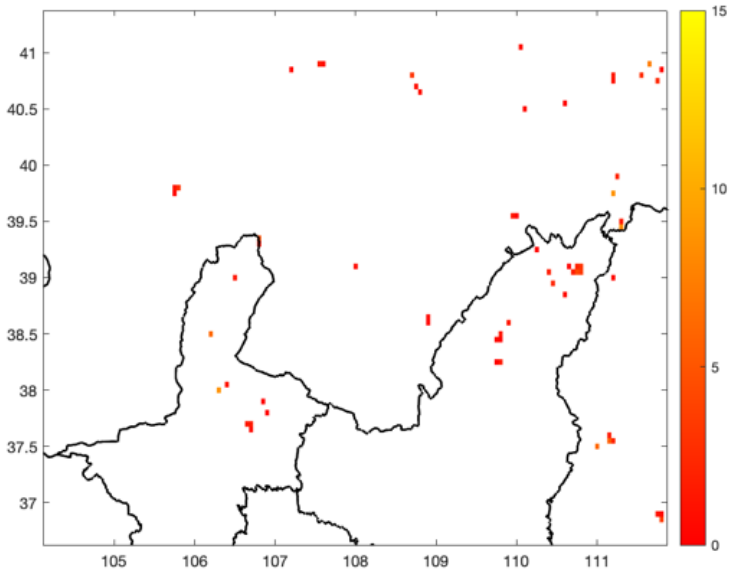

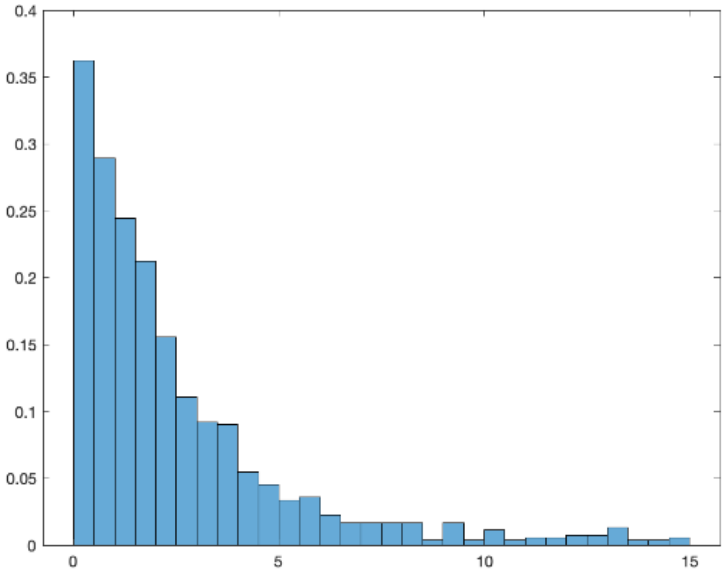

Figure 3: Computed values of: (top row) climatological map and month-by-month PDF of $\alpha_1[NO_x/NO_2]$; (second row) climatological map and month-by-month PDF of α_2[days]; (third row) climatological map and month-by-month PDF of α_3 out from sources [km]; and (fourth row) climatological map and month-by-month PDF of α_3 in to sources [km].

When the values of α_1, α_2, and α_3 are used to compute the emissions, first statistical samples of α_1, α_2, and α_3 are repeated 1000 times using a bootstrap approach based on a random sampling from each respective PDF, within the ranges given in Figure 3. The equations are integrated using the TROPOMI NO_2 columns, a priori emissions, and meteorology such that it is temporally and spatially consistent, using all days of data available where data exists on the day being computed, either the day before or after (for the time gradient), on the same day being computed at least one surrounding grid (for the horizontal gradient), and in combination with the sampled values of α_1, α_2, and α_3 having an available best fit value during the respective month. For grids with data and with a set of α_1, α_2, and α_3 the bootstrap approach is used, while for grids with existing α_1, α_2, and α_3 only these values are used.

3. Results

The 2019 annual mean of daily NO_2 column loading and its probability distribution function [PDF], and the annual standard deviation of daily NO_2 columns (post-filtered for signals smaller than the measurement uncertainty) and its PDF are mapped in (Figure 4), provide a quantitative measure of the signal's climatology and variability (Cohen, 2014; Lin et al., 2020; Stavrakou et al., 2016; Verhoelst et al., 2021). High average values with a relatively low normalized standard deviation are observed in known urban and coal consuming areas, consistent with well characterized and regulated sources (Lin et al., 2020). Data with a moderately high NO_2 column and moderately high normalized standard deviation are observed in suburban areas as well as in some outlying areas far from existing energy, steel, and chemical factories, including in locations completely removed from substantial or village level administrative regions (Deng et al., 2021). Such combination of mean and standard deviation has been previously observed in biomass burning regions, which are not prevalent in the region of this study, and therefore likely indicate an anthropogenic source undergoing rapid change or otherwise mis-identified or mis-characterized (Wang et al., 2021a).

Figure 4: TROPOMI daily average climatological NO_2column loading [10^{15} molec/cm^2]: (top left) mean, (top right) PDF of mean, (bottom left) standard deviation, and (bottom right) PDF of standard deviation.

The mass conservation equation for NO_x in-situ is a function of column NO_2 measurements via the linear transformation NO_x=$\alpha_1 NO_2$, consistent with the fact that after emission, the ratio of NO_2 to NO_x achieves a rapid local pseudo-steady state equilibrium (Mavroidis and Chaloulakou, 2011) and that NO isn't readily measurable via remote sensing. This assumption has been adapted as a fixed value by the emissions and chemical modeling communities with a range of values from 9 to 19 (Oliver et al., 1994; van Amstel et al., 1999), while in this work, the value of α_1 is allowed to vary based on the best fit between the measurements, meteorology, and the a priori emissions data, allowing for an optimal range of values that is still thermodynamically realistic (Chong et al., 2010). Post-transformation, mass conservation equation is based on measurements of NO_2, as given in Equation 1a. Equation 1a is rearranged to Equation 1b to solve for the emissions of NO_x [E_{NOx}], where $\alpha_2$represents chemical decay of NO_x and $\alpha_3$represents the advective and pressure transport of NO_x.

$$d(\alpha_1[NO_2])/dt = E_{NOx} + \alpha_2(\alpha_1[NO_2]) + \alpha_3[?](u\alpha_1[NO_2]) \quad (1a)$$

$$E_{NOx} = \alpha_1 d([NO_2])/dt - \alpha_2\alpha_1[NO_2] - \alpha_3\alpha_1[?](u[NO_2]) \quad (1b)$$

3.1 Emissions Drivers

The terms completely govern the mass-balance of NO_x: (a) the scaled change in measured NO_2 between the previous day's and present day's measurements, (b) the present day's a priori emissions [for fitting] or computed MCMFE-NO_x[prediction], (c) the scaled change in the present day's measurement due to chemical decay, (d) the scaled change in the present day's measurement due to horizontal advection in or out of the geographic location, and (e) the scaled change in the present day's measurement due to the squeezing or thinning of air at the geographic location. The final assumption is that NO_x emissions are roughly uniform throughout the day, allowing the integrated net effect of those processes with an effect faster than the one-day time step to be representative throughout the day, a reasonable assumption on the scales being analyzed in this work (Cohen and Prinn, 2011; He et al., 2020).

PDFs of the best fit values of α_1, α_2, and α_3 (Figure 3) are constrained by idealized and field measurements, allowing for greater variability than many current models provide, while still being consistent with real world conditions (Laughner and Cohen, 2019). The 30%, median, and 70% values of α_1 are 9.6, 16.9, and 29.2 respectively, covering the range used by community models, but with a wider range on the high side (less NO_2 in NO_x), consistent with higher temperature combustion associated with ever-increasing energy efficiency of coal boilers (Cox, 1999; van Der A et al., 2008). The 30%, median, and 70% values of α_2 are -0.076days, -0.089days, and -0.11days respectively, covering the range of values in community models, but with a wider range on the negative side (faster chemical reactivity) consistent with theory and measurements in other similar geographic regions, which are both at higher elevation and which tend to be relatively cloud free (Beirle et al., 2011; Laughner and Cohen, 2019). The 72% of cases in which the transport is negative (net export) have a 30%, median, and 70% values of α_3 of -1.8km, -3.5km, and -6.0km respectively, while the 28% of cases in which transport is positive (net import) have a 30%, median, and 70% values of α_3/α_1 of 0.9km, 1.7km, and 3.2km. These values include values of fluxes advected into source emitting regions, something that current models do not represent well but is known to exist from observations, as well as slightly smaller than current modeled transport exported from emitting regions into remote downwind regions (Aouizerats et al., 2015; Cohen et al., 2011; Lee et al., 2017).

Figure 5: Representations of daily computed MCMFE-NO_x[$\mu g/m^2 s$]: (a) climatological mean, (b) climatological standard deviation, and (c) histograms of all daily data (blue), and of the grid-by-grid climatological mean data (red).

3.2 Emissions See-Saw

Equation 1b is solved daily by sampling from the respective monthly PDFs of α_1, α_2, and α_3, TROPOMI NO_2

and reanalysis wind. The annual mean and standard deviation of the daily emissions are given in (Figure 5) with the day-to-day results available for download at https://www.doi.org/10.6084/m9.figshare.19560517. Emissions cover 35% of the spatial domain, with an average daily value of 1.1±1.0μg/m^{2}s, as compared with the a priori which covers 14% of the domain and has a mean value of 0.78±1.7μg/m^{2}s.

The majority of the increase in emissions occurs in grids with low a priori emissions (hereafter defined as <1.1μg/m^{2}s), with MCMFE-NO$_x$computed to be 1.2±0.44μg/m^{2}s compared to the a priori emissions of 0.22±0.26μg/m^{2}s, consistent with new and increasing small and moderate sources (Figure 6). Oppositely, on those grids with a high a priori emissions (hereafter defined as >1.1μg/m^{2}s), MCMFE-NO$_x$are found to be slightly lower at 2.7±2.4μg/m^{2}s compared to the a priori emissions 3.0±2.7μg/m^{2}s, consistent with a slow but continuous reduction in emissions from known and well-regulated sources such as urban centers and large steel, chemical and power plants. These findings are consistent with recent laws in China targeting controls at well-known sites to bring them under stricter compliance.

MCMFE-NO$_x$ over grids without a priori data (newly identified sources) has a low value of 0.95±0.42μg/m^{2}s and covers 27% of the domain. Conversely, grids which contain a priori emissions without MCMFE-NO$_x$ (well-controlled sources) yield a result with a low average and high variance value of 0.68±1.6μg/m^{2}s and cover 14% of the domain, demonstrating a large amount of variability. Thus, heavily polluting sites have emissions consistent with increasing energy efficiency, successfully abated or mitigated NO$_x$ sources, and/or have been possibly shut down, while at the same time a large number of small and medium emitting sites are more active than before, new, or were previously mis-identified.

Figure 6: Difference between MCMFE-NO$_x$[μg/m^{2}s] and: (a) MEIC (when between 0.3μg/m^{2}s and 1.1μg/m^{2}s), (b) MEIC (when less than 0.3μg/m^{2}s), and (c) MEIC (when larger than 1.1μg/m^{2}s). (d) PDFs of cases (a) blue, (b) red, and (c) orange.

Integrating over the domain MCMFE-NO$_x$ is 1.90Mton/yr, compared with the a priori net emissions of 1.10Mton/yr. MCMFE-NO$_x$ in newly identified areas is 1.18Mton/yr, and MCMFE-NO$_x$ in grids with a low a priori is 0.47Mton/yr, compared with the a priori total over low regions of 0.26Mton/yr. MCMFE-NO$_x$ in highly emitting areas including urban centers, major coal fired power plants, chemistry plants, and steel plants is 0.24Mton/yr, compared to the a priori emissions of 0.85Mton/yr.

3.3 Comparison with EPA Emissions

On the 56 grids which have emissions computed using an independent stack-based concentration measurement approach at power plants, steel plants, and coal to chemicals plants [CEMS] that overlap with MCMFE-NO$_x$ grids, the average emissions are 2.1±2.1μg/m^{2}s and 1.2±0.98μg/m^{2}s respectively (Figure 7). The match is closer between the 25 MCMFE-NO$_x$ grids which do not contain a priori emissions 1.1±0.38μg/m^{2}s and CEMS 1.1±0.58μg/m^{2}s, than between the 12 grids at which all of MCMFE-NO$_x$ 1.3±0.41μg/m^{2}s, CEMS 1.0±0.48μg/m^{2}s, and the a priori emissions 0.43±0.28μg/m^{2}s all overlap. On the 51 grids where a priori emissions overlap with CEMS, the a priori emissions 2.7±3.0μg/m^{2}s has less overlap with CEMS 1.0±1.1μg/m^{2}s than the 56 grid overlap between CEMS and MCMFE-NO$_x$. Furthermore, the 11 grids where a priori emissions overlap with CEMS and do not have any MCMFE-NO$_x$ data, the difference between the a priori 3.5±3.0μg/m^{2}s and CEMS 1.0±0.71μg/m^{2}s is larger still. These results clearly demonstrate that MCMFE-NO$_x$ has a closer fit to and less bias with respect to CEMS than the a priori.

Figure 7: Comparison of annual emissions (bars) and 1 standard deviation uncertainty ranges (lines) for the following cases: (a) 25 sites which overlap between MCMFE-NO$_x$ (blue) and CEMS (red), (b) 11 sites which overlap between the a priori (blue) and CEMS (red), and (c) 12 sites which overlap between MCMFE-NO$_x$ (blue), CEMS (red), and the a priori (orange). (d) Map of the difference in emissions given in (a).

4. Discussion

The emissions computed using daily NO_2 measurements and the 4-term mass conservation approach are 1.7

times higher than emissions from the gold-standard bottom-up inventory. However, there is a clear difference in geography and two contributing factors. First, emissions in known urban centers and large coal consuming areas (Yinchuan, Baotao, Wuhai, and Yulin) are 28% of the a priori value. Second, emissions in regions with a low a priori or no a priori emissions, specifically with new or growing chemical industries (Xiaoyi and expansion around Yinchuan and Yulin), new coal-based powerplants (expansion around Wuhai), new steel production (expansion outside of and around Baotou), and regions with new or significantly expanding urban cores (Huhehaote and Eredosi) have a computed emissions 250% the a priori value. This see-saw of increasing emissions in rapidly changing areas combined with decreasing emissions in more established, closely monitored, and more regulated regions, is consistent with the rapid economic development, population shifts, and policies implemented. Furthermore, the emissions match better with independent stack-based measurements of emissions, overall, as well as in terms of the conclusions above: the lower emitting stacks tend to have a slightly higher total emissions from MCMFE-NO_x, consistent with other sources associated with the activity present at the stack sites, while the higher emitting stacks tend to have a lower total emissions from MCMFE-NO_x, still larger than the stack values themselves, but only barely, again consistent with increased regulation. MCMFE-NO_x also identifies new sources including new or growing small-scale industry, biomass and agricultural burning, and residential sources, and in particular fits the stack-based emissions much better in regions without a priori emissions.

4.1 Gleaning Information about Combustion, Chemistry, and Transport

There is a significant number of grids which are have an emissions ratio of NO_x/NO_2 outside of the range used in chemical transport models, yet still consistent with thermodynamics and observation studies, indicating that this result accounts for more real-world variability (Mavroidis and Chaloulakou, 2011; Oliver et al., 1994; van Amstel et al., 1999). The large value of $\alpha_1$around Wuhai and Baotou is consistent with increased NO occurring at higher temperature combustion conditions, consistent with the increased energy efficiency of thermal power plants and steel production sites. The small value of α_1 in Xiaoyi, Yinchuan, and Ningdong is consistent with less efficient and lower temperature combustion conditions associated with coal to chemical plants, residential, and transportation sources. The generally more negative values of α_2 are consistent with faster chemistry than currently used in the modeling community (Laughner and Cohen, 2019), but are consistent with observations in regions with higher amounts of surface UV irradiance, consistent with the geography of the region studied here (Cadet et al., 2020). The magnitude of α_3 is observed to provide a significant amount of NO_x transport over 44 continuous grids around Baotou and 22 continuous grids around Wuhai, in contrast to most studies indicating little long-range transport. The results are consistent with proximity to mountains being one major driving factor (Bonasoni et al., 2010). Interestingly $\alpha_3$has a positive value over 5 continuous grids in Eerduosi, indicating transport does contribute to NO_x in some urban areas, a significant break with traditional assumptions that boundary layer height, local emissions, and wind speed control sources in urban centers, but consistent with idealized studies (Cohen and Prinn, 2011; Cohen et al., 2011). Hence MCMFE-NO_x can quantify the contributions on NO_x emissions and loadings based on source thermodynamics and efficiency, chemical and radiative conditions, atmospheric properties, measurement uncertainty, and even topography.

4.2 Limitations and Applications

There are at least three limitations in this work. The remotely sensed dataset analyzed in this work has daily data over 1 year at a spatial resolution of 3.5km×7/5.5km, meaning studies requiring higher resolution or similar resolution at longer time-scales cannot be made. Secondly, the region analyzed is relatively homogenous in terms of sources, geography, and a priori emissions, and therefore this approach may not work well in a region which is more heterogenous in terms of emissions sources, geographic conditions, and other phenomena impacting the remotely sensed retrievals. Furthermore, the chemical decay and transport are both limited to first-order processes, which may not work well under highly polluted conditions, or in the case of a large number of individual sources in close geographic proximity, requiring further enhancements to the mass-conserving equations in these regions to better account for non -linear effects.

Applications focusing on expanding the procedure to other rapidly changing source regions, extending the

analysis over longer period of time, and using a greater number of a priori emissions sources would all be logical next steps. Expanding the values obtained to other global regions which are climatologically and technologically similar but located in different regions of the world would also make for impactful follow-up. Furthermore, expanding into regions with few or no a priori emissions inventories could add further value. Additionally, analysis using smarter sampling and fitting could also lead to an increase in the robustness of the solution. On top of this, working iteratively with the bottom-up emissions community to adapt these emissions datasets, and then using the enhanced a priori datasets to re-drive this process could provide tighter uncertainty bounds and reduce biases. Finally, this method could be used by the air pollution control community to rapidly identify and/or predict specific extreme air pollution events.

Description of author's responsibilities

This work was conceptualized by Jason Blake Cohen and Kai Qin. The methods were developed by Jason Blake Cohen and Kai Qin. Investigation was done by Jincheng Shi, Kai Qin, and Jason Blake Cohen. Visualizations were made by He Qin, Jincheng Shi, and Jason Blake Cohen. Writing of the original draft was done by Kai Qin, Jason Blake Cohen, Jincheng Shi, He Qin, Shuo Wang, Jian Liu, and Weizhi Deng. Writing at the review and editing stages were done by Kai Qin and Jason Blake Cohen.

Funding

This work was supported by the National Natural Science Foundation of China [Grant Numbers 42075147, 41975041]; Shanxi Province Major Science and Technique Program [Grant Number 202101090301013]; and the Major research project of Jiangsu Key Laboratory of Coal-based Greenhouse Gas Control and Utilization [Grant Number 2020ZDZZ03A].

Data Statement

All data presented in and underlying the figures, the daily gridded MCMFE-NO_x emissions, and the computed monthly gridded values of α_1, α_2, and $\alpha_3$are free for download at: https://www.doi.org/10.6084/m9.figshare.19560517. The TROPOMI data used in this work is available for download at: https://sentinel.esa.int/documents/247904/ 2476257/Sentinel-5P-TROPOMI-ATBD-NO2-data-products.

References

Aamaas, B., Berntsen, T. K., Fuglestvedt, J. S., Shine, K. P., & Collins, W. J. (2017). Regional temperature change potentials for short-lived climate forcers based on radiative forcing from multiple models, *Atmos. Chem. Phys.* , 17, 10795–10809.

Alvarado, M. J., Logan, J. A., Mao, J., Apel, E., Riemer, D., Blake, D., ... & Sager, P. L. (2010). Nitrogen oxides and PAN in plumes from boreal fires during ARCTAS-B and their impact on ozone: an integrated analysis of aircraft and satellite observations. *Atmospheric Chemistry and Physics* , *10* (20), 9739-9760.

Aouizerats, B., Van Der Werf, G. R., Balasubramanian, R., & Betha, R. (2015). Importance of transboundary transport of biomass burning emissions to regional air quality in Southeast Asia during a high fire event. *Atmospheric chemistry and Physics* , *15* (1), 363-373.

Beirle, S., Boersma, K. F., Platt, U., Lawrence, M. G., & Wagner, T. (2011). Megacity emissions and lifetimes of nitrogen oxides probed from space. *Science* , *333* (6050), 1737-1739.

Beirle, S., Borger, C., Dörner, S., Li, A., Hu, Z., Liu, F., ... & Wagner, T. (2019). Pinpointing nitrogen oxide emissions from space.*Science advances* , *5* (11), eaax9800.

Bonasoni, P., Laj, P., Marinoni, A., Sprenger, M., Angelini, F., Arduini, J., Bonafè, U., Calzolari, F., Colombo, T., Decesari, S., Di Biagio, C., di Sarra, A. G., Evangelisti, F., Duchi, R., Facchini, MC., Fuzzi, S., Gobbi, G. P., Maione, M., Panday, A., Roccato, F., Sellegri, K., Venzac, H., Verza, GP., Villani, P., Vuillermoz, E., and Cristofanelli, P. (2010) Atmospheric Brown Clouds in the Himalayas: first two years of continuous observations at the Nepal Climate Observatory-Pyramid (5079 m). *Atmos. Chem. Phys., 10* , 7515–7531.

Brewer, A. W., McElroy, C. T., & Kerr, J. B. (1973). Nitrogen dioxide concentrations in the atmosphere. *Nature* , *246* (5429), 129-133.

Cadet, J. M., Bencherif, H., Cadet, N., Lamy, K., Portafaix, T., Belus, M., Brogniez, C., Auriol, F., Metzger, J.M., & Wright, C.Y. (2020) Solar UV Radiation in the Tropics: Human Exposure at Reunion Island (21 degrees S, 55 degrees E) during Summer Outdoor Activities. *Int J Environ Res Public Health* , *17* (21), 8105.

Chen, T. M., Kuschner, W. G., Gokhale, J., & Shofer, S. (2007). Outdoor air pollution: nitrogen dioxide, sulfur dioxide, and carbon monoxide health effects. *The American journal of the medical sciences* ,*333* (4), 249-256.

Chen, W., Li, H., & Wu, Z. (2010). Western China energy development and west to east energy transfer: Application of the Western China Sustainable Energy Development Model. *Energy Policy* ,*38* (11), 7106-7120.

Chong, J. J., Tsolakis, A., Gill, S. S., Theinnoi, K., & Golunski, S. E. (2010). Enhancing the NO_2/NO_x ratio in compression ignition engines by hydrogen and reformate combustion, for improved aftertreatment performance. *International Journal of Hydrogen Energy* , *35* (16), 8723-8732.

Cohen, J. B. (2014) Quantifying the Occurrence and Magnitude of the Southeast Asian Fire Climatology. *Environmental Research Letters* , 9, 114018.

Cohen, J. B., & Prinn, R. G. (2011). Development of a fast, urban chemistry metamodel for inclusion in global models. *Atmospheric Chemistry and Physics* , *11* (15), 7629-7656.

Cohen, J. B., & Wang, C. (2014). Estimating global black carbon emissions using a top-down Kalman Filter approach. *Journal of Geophysical Research: Atmospheres* , *119* (1), 307-323.

Cohen, J. B., Prinn, R. G., & Wang, C. (2011). The impact of detailed urban-scale processing on the composition, distribution, and radiative forcing of anthropogenic aerosols. *Geophysical Research Letters* ,*38* (10).

Collins, W. J., Fry, M. M., Yu, H., Fuglestvedt, J. S., Shindell, D. T., and West, J. J. (2013) Global and regional temperature-change potentials for near-term climate forcers, *Atmos. Chem. Phys.* , 13, 2471–2485.

Cox, L. (1999). Nitrogen oxides (NOx) why and how they are controlled.*Diane Publishing* .

Crutzen, P. J. (1970). The influence of nitrogen oxides on the atmospheric ozone content. *Quarterly Journal of the Royal Meteorological Society* , *96* (408), 320-325.

de Foy, B., Wilkins, J. L., Lu, Z., Streets, D. G., & Duncan, B. N. (2014). Model evaluation of methods for estimating surface emissions and chemical lifetimes from satellite data. *Atmospheric Environment* ,*98* , 66-77.

Deng, W., Cohen, J. B., Wang, S., & Lin, C. (2021). Improving the understanding between climate variability and observed extremes of global NO_2 over the past 15 years. *Environmental Research Letters* , *16* (5), 054020.

Drysdale, W. S., Vaughan, A. R., Squires, F. A., Cliff, S. J., Metzger, S., Durden, D., ... & Lee, J. D. (2022). Eddy Covariance Measurements Highlight Sources of Nitrogen Oxide Emissions Missing from Inventories for Central London. *Atmospheric Chemistry and Physics Discussions* , 1-35.

Evangeliou, N., Thompson, R. L., Eckhardt, S., & Stohl, A. (2018). Top-down estimates of black carbon emissions at high latitudes using an atmospheric transport model and a Bayesian inversion framework, Atmos. Chem. Phys., 18, 15307–15327.

Geddes, J. A., & Murphy, J. G. (2014). Observations of reactive nitrogen oxide fluxes by eddy covariance above two midlatitude North American mixed hardwood forests. *Atmospheric Chemistry and Physics* , *14* (6), 2939-2957.

Haszpra, L., Hidy, D., Taligas, T., & Barcza, Z. (2018). First results of tall tower based nitrous oxide flux monitoring over an agricultural region in Central Europe. *Atmospheric Environment* , *176* , 240-251.

He, Q., Qin, K., Cohen, J. B., Loyola, D., Li, D., Shi, J., & Xue, Y. (2020). Spatially and temporally coherent reconstruction of tropospheric NO_2 over China combining OMI and GOME-2B measurements.*Environmental Research Letters* , *15* (12), 125011.

Henderson, B. H., Pinder, R. W., Crooks, J., Cohen, R. C., Carlton, A. G., Pye, H. O. T., & Vizuete, W. (2012). Combining Bayesian methods and aircraft observations to constrain the HO + NO_2 reaction rate. *Atmospheric Chemistry and Physics* , *12* (2), 653-667.

Holmes, C. D., Prather, M. J., Sovde, O. A., & Myhre, G. (2013) Future methane, hydroxyl, and their uncertainties: key climate and emission parameters for future predictions, *Atmos. Chem. Phys.* , 13, 285–302.

Hu, Y.; Zang, Z.; Chen, D.; Ma, X.; Liang, Y.; You, W.; Pan, X.; Wang, L.; Wang, D.; Zhang, Z. (2022) Optimization and Evaluation of SO2 Emissions Based on WRF-Chem and 3DVAR Data Assimilation. *Remote Sens.* 14, 220.

Jacob, D. J., Heikes, E. G., Fan, S. M., Logan, J. A., Mauzerall, D. L., Bradshaw, J. D., ... & Sachse, G. W. (1996). Origin of ozone and NOx in the tropical troposphere: A photochemical analysis of aircraft observations over the South Atlantic basin. *Journal of Geophysical Research: Atmospheres* , *101* (D19), 24235-24250.

Jin, X., Zhu, Q., & Cohen, R. C. (2021). Direct estimates of biomass burning NO_x emissions and lifetimes using daily observations from TROPOMI. *Atmospheric Chemistry and Physics* ,*21* (20), 15569-15587.

Karl, T., Graus, M., Striednig, M., Lamprecht, C., Hammerle, A., Wohlfahrt, G., ... & Lee, J. (2017). Urban eddy covariance measurements reveal significant missing NOx emissions in Central Europe.*Scientific reports* , *7* (1), 1-9.

Karplus, V. J., Zhang, S., & Almond, D. (2018). Quantifying coal power plant responses to tighter SO_2 emissions standards in China. *Proceedings of the National Academy of Sciences* ,*115* (27), 7004-7009.

Kong, H., Lin, J., Chen, L., Zhang, Y., Yan, Y., Liu, M., Ni, R., Liu, Z., and Weng, H. (2022). Considerable Unaccounted Local Sources of NOx Emissions in China Revealed from Satellite. *Environmental Science & Technology* , 2022 56 (11), 7131-7142.

Laughner, J., & Cohen, R. (2019). Direct observation of changing NO_x lifetime in North American cities. *Science* ,*366* (6466), 723-727.

Lee, H. H., Bar-Or, R. Z., & Wang, C. (2017). Biomass burning aerosols and the low-visibility events in Southeast Asia. *Atmospheric Chemistry and Physics* , *17* (2), 965-980.

Lee, J. D., Helfter, C., Purvis, R. M., Beevers, S. D., Carslaw, D. C., Lewis, A. C., ... & Nemitz, E. G. (2015). Measurement of NOx fluxes from a tall tower in central London, UK and comparison with emissions inventories. *Environmental science & technology* , *49* (2), 1025-1034.

Lei Z., Jacob, D., Mickley, L., Marais, E., Cohan, D., Yoshida, Y., Duncan, B., Gonzalez, & Chance, K. (2014) Anthropogenic emissions of highly reactive volatile organic compounds in eastern Texas inferred from oversampling of satellite (OMI) measurements of HCHO columns.*Environ. Res. Lett.* , 9, 114004.

Li, L., Hoffmann, M. R., & Colussi, A. J. (2018). Role of nitrogen dioxide in the production of sulfate during Chinese haze-aerosol episodes. *Environmental science & technology* , *52* (5), 2686-2693.

Li, M., Zhang, Q., Kurokawa, J. I., Woo, J. H., He, K., Lu, Z., ... & Zheng, B. (2017). MIX: a mosaic Asian anthropogenic emission inventory under the international collaboration framework of the MICS-Asia and HTAP. *Atmospheric Chemistry and Physics* , *17* (2), 935-963.

Liang, X., Huang, T., Lin, S., Wang, J., Mo, J., Gao, H., ... & Ma, J. (2019). Chemical composition and source apportionment of PM_1 and $PM_{2.5}$ in a national coal chemical industrial base of the Golden Energy Triangle, Northwest China. *Science of the Total Environment* , *659* , 188-199.

Lin, C., Cohen, J. B., Wang, S., Lan, R., & Deng, W. (2020). A new perspective on the spatial, temporal, and vertical distribution of biomass burning: quantifying a significant increase in CO emissions. *Environmental Research Letters* , *15* (10), 104091.

Lin, J. T., Liu, Z., Zhang, Q., Liu, H., Mao, J., & Zhuang, G. (2012). Modeling uncertainties for tropospheric nitrogen dioxide columns affecting satellite-based inverse modeling of nitrogen oxides emissions. *Atmospheric Chemistry and Physics* , *12* (24), 12255-12275.

Ling, Z., Huang, T., Zhao, Y., Li, J., Zhang, X., Wang, J., ... & Ma, J. (2017). OMI-measured increasing SO_2 emissions due to energy industry expansion and relocation in northwestern China. *Atmospheric Chemistry and Physics* , *17* (14), 9115-9131.

Liu, M., Lin, J., Kong, H., Boersma, K. F., Eskes, H., Kanaya, Y., ... & Wang, J. (2020). A new TROPOMI product for tropospheric NO_2 columns over East Asia with explicit aerosol corrections. *Atmospheric Measurement Techniques* , *13* (8), 4247-4259.

Logan, J. A. (1983). Nitrogen oxides in the troposphere: Global and regional budgets. *Journal of Geophysical Research: Oceans* ,*88* (C15), 10785-10807.

Lueue, C., Wenig, M., Wagner, T., Klimm, O., Platt, U., & Jahne, B. (2001). Quantitative analysis of NO_x emissions from Global Ozone Monitoring Experiment satellite image sequences. *Journal of Geophysical Research: Atmospheres* ,*106* (D6), 5493-5505.

Lund, M. T., Aamaas, B., Stjern, C. W., Klimont, Z., Berntsen, T. K., & Samset, B. H. (2020). A continued role of short-lived climate forcers under the Shared Socioeconomic Pathways. *Earth Syst. Dynam.* , 11, 977–993.

Martin, R. V., Jacob, D. J., Chance, K., Kurosu, T. P., Palmer, P. I., & Evans, M. J. (2003). Global inventory of nitrogen oxide emissions constrained by space-based observations of NO_2 columns. *Journal of Geophysical Research: Atmospheres* , *108* (D17).

Martin, R. V., Sioris, C. E., Chance, K., Ryerson, T. B., Bertram, T. H., Wooldridge, P. J., ... & Flocke, F. M. (2006). Evaluation of space-based constraints on global nitrogen oxide emissions with regional aircraft measurements over and downwind of eastern North America. *Journal of Geophysical Research: Atmospheres* , *111* (D15).

Mavroidis, I., & Chaloulakou, A. (2011). Long-term trends of primary and secondary NO_2production in the Athens area. Variation of the NO_2/NO_x ratio. *Atmospheric environment* , *45* (38), 6872-6879.

Mijling, B., Van Der A, R. J., & Zhang, Q. (2013). Regional nitrogen oxides emission trends in East Asia observed from space. *Atmospheric Chemistry and Physics* , *13* (23), 12003-12012.

Monks, P. S., Archibald, A. T., Colette, A., Cooper, O., Coyle, M., Derwent, R., Fowler, D., Granier, C., Law, K. S., Mills, G. E., Stevenson, D. S., Tarasova, O., Thouret, V., von Schneidemesser, E., Sommariva, R., Wild, O., and Williams, M. L. (2015) Tropospheric ozone and its precursors from the urban to the global scale from air quality to short-lived climate forcer, *Atmos. Chem. Phys.* , 15, 8889–8973.

Napelenok, S. L., Pinder, R. W., Gilliland, A. B., & Martin, R. V. (2008). A method for evaluating spatially-resolved NO_xemissions using Kalman filter inversion, direct sensitivities, and space-based NO_2 observations. *Atmospheric Chemistry and Physics* , *8* (18), 5603-5614.

Olivier, J. G. J., Bouwman, A. F., Van der Maas, C. W. M., & Berdowski, J. J. M. (1994). Emission database for global atmospheric research (EDGAR). *Environmental Monitoring and Assessment* , 31(1), 93-106.

Platz, J., Nielsen, O. J., Wallington, T. J., Ball, J. C., Hurley, M. D., Straccia, A. M., ... & Sehested, J. (1998). Atmospheric chemistry of the phenoxy radical, C6H5O (*): UV spectrum and kinetics of its reaction with NO, NO_2, and O_2. *The Journal of Physical Chemistry A* , *102* (41), 7964-7974.

Rogelj, J., Schaeffer, M., Meinshausen, M., Shindell, D., Hare, W., Klimont, Z., Velders, G., Amann, M., & Schellnhuber, H. (2014). Disentangling the effects of CO2 and short-lived climate forcer mitigation. *Proceedings of the National Academy of Sciences* , 111, 46, 16325-16330.

Rollins, A. W., Browne, E. C., Min, K. E., Pusede, S. E., Wooldridge, P. J., Gentner, D. R., ... & Cohen, R. C. (2012). Evidence for NOx control over nighttime SOA formation. *Science* , *337* (6099), 1210-1212.

Sand, M., Berntsen, T., von Salzen, K. et al. (2016) Response of Arctic temperature to changes in emissions of short-lived climate forcers.*Nature Clim Change* , 6, 286–289.

Seinfeld, J. H. (1989). Urban air pollution: state of the science.*Science* , *243* (4892), 745-752.

Shen, Y., Zhang, X., Brook, J. R., Huang, T., Zhao, Y., Gao, H., & Ma, J. (2016). Satellite remote sensing of air quality in the Energy Golden Triangle in Northwest China. *Environmental Science & Technology Letters* , *3* (7), 275-279.

Shindell, D. T. et al. Simultaneously mitigating near-term climate change and improving human health and food security. *Science* , 335, 183–189 (2012).

Stavrakou, T., Muller, J. F., Bauwens, M., De Smedt, I., Lerot, C., Van Roozendael, M., ... & Song, Y. (2016). Substantial underestimation of post-harvest burning emissions in the North China Plain revealed by multi-species space observations. *Scientific Reports* ,*6* (1), 1-11.

Stavrakou, T., Muller, J. F., Boersma, K. F., De Smedt, I., & Van Der A, R. J. (2008). Assessing the distribution and growth rates of NO_x emission sources by inverting a 10-year record of NO_2 satellite columns. *Geophysical Research Letters* , *35* (10).

Stavrakou, T., Muller, J. F., Boersma, K. F., Van Der A, R. J., Kurokawa, J., Ohara, T., & Zhang, Q. (2013). Key chemical NO_x sink uncertainties and how they influence top-down emissions of nitrogen oxides. *Atmospheric Chemistry and Physics* ,*13* (17), 9057-9082.

Streets, D. G., & Waldhoff, S. T. (2000). Present and future emissions of air pollutants in China: SO_2, NO_x, and CO. *Atmospheric Environment* , *34* (3), 363-374.

Tan, Z., Lu, K., Dong, H., Hu, M., Li, X., Liu, Y., ... & Zhang, Y. (2018). Explicit diagnosis of the local ozone production rate and the ozone-NOx-VOC sensitivities. *Science bulletin* , *63* (16), 1067-1076.

Tang, L., Xue, X., Qu, J., Mi, Z., Bo, X., Chang, X., ... & Dong, G. (2020). Air pollution emissions from Chinese power plants based on the continuous emission monitoring systems network. *Scientific Data* , *7* (1), 1-10.

Tong, Z., Li, Y., Lin, Q., Wang, H., Zhang, S., Wu, Y., & Zhang, K. M. (2022). Uncertainty investigation of plume-chasing method for measuring on-road NO_x emission factors of heavy-duty diesel vehicles. *Journal of Hazardous Materials* , *424* , 127372.

van Amstel, A., Olivier, J., & Janssen, L. (1999). Analysis of differences between national inventories and an Emissions Database for Global Atmospheric Research (EDGAR). *Environmental Science & Policy* , *2* (3), 275-293.

van der A, R. J., de Laat, A. T. J., Ding, J., & Eskes, H. J. (2020). Connecting the dots: NOx emissions along a West Siberian natural gas pipeline. *npj Climate and Atmospheric Science* , *3* (1), 1-7.

van Der A, R. J., Eskes, H. J., Boersma, K. F., Van Noije, T. P. C., Van Roozendael, M., De Smedt, I., ... & Meijer, E. W. (2008). Trends, seasonal variability and dominant NOx source derived from a ten year record of NO2 measured from space. *Journal of Geophysical Research: Atmospheres* , *113* (D4).

Van Geffen, J., Boersma, K. F., Eskes, H., Sneep, M., Ter Linden, M., Zara, M., & Veefkind, J. P. (2020). S5P TROPOMI NO_2slant column retrieval: method, stability, uncertainties and comparisons with OMI. *Atmospheric Measurement Techniques* , *13* (3), 1315-1335.

Vaughan, A. R., Lee, J. D., Misztal, P. K., Metzger, S., Shaw, M. D., Lewis, A. C., ... & Karl, T. G. (2016). Spatially resolved flux measurements of NO_x from London suggest significantly higher emissions than predicted by inventories. *Faraday discussions* , *189* , 455-472.

Veefkind, J. P., Aben, I., McMullan, K., Forster, H., De Vries, J., Otter, G., ... & Levelt, P. F. (2012). TROPOMI on the ESA Sentinel-5 Precursor: A GMES mission for global observations of the atmospheric composition for climate, air quality and ozone layer applications.*Remote sensing of environment* , *120* , 70-83.

Verhoelst, T., Compernolle, S., Pinardi, G., Lambert, J. C., Eskes, H. J., Eichmann, K. U., ... & Zehner, C. (2021). Ground-based validation of the Copernicus Sentinel-5p TROPOMI NO_2 measurements with the NDACC ZSL-DOAS, MAX-DOAS and Pandonia global networks.*Atmospheric Measurement Techniques* , *14* (1), 481-510.

Wang, S., Cohen, J. B., Deng, W., Qin, K., & Guo, J. (2021). Using a New Top-Down Constrained Emissions Inventory to Attribute the Previously Unknown Source of Extreme Aerosol Loadings Observed Annually in the Monsoon Asia Free Troposphere. *Earth's Future* , *9* (7), e2021EF002167.

Wang, S., Streets, D. G., Zhang, Q., He, K., Chen, D., Kang, S., ... & Wang, Y. (2010). Satellite detection and model verification of NO_x emissions from power plants in Northern China.*Environmental Research Letters* , *5* (4), 044007.

Wang, S. W., Zhang, Q., Streets, D. G., He, K. B., Martin, R. V., Lamsal, L. N., ... & Lu, Z. (2012). Growth in NOx emissions from power plants in China: bottom-up estimates and satellite observations.*Atmospheric Chemistry and Physics* , *12* (10), 4429-4447.

Zhang, X., & Schreifels, J. (2011). Continuous emission monitoring systems at power plants in China: Improving SO_2 emission measurement. *Energy Policy* , *39* (11), 7432-7438.

Zhao, C., & Wang, Y. (2009). Assimilated inversion of NO_x emissions over east Asia using OMI NO_2 column measurements. *Geophysical Research Letters* , *36* (6).

Zheng, Y. & Unger, N. (2021). Reducing planetary health risks through short-lived climate forcer mitigation. *GeoHealth* , 5, e2021GH000422

Zyrichidou, I., Koukouli, M. E., Balis, D., Markakis, K., Poupkou, A., Katragkou, E., ... & Van Roozendael, M. (2015). Identification of surface NO_x emission sources on a regional scale using OMI NO_2. *Atmospheric Environment* , *101* , 82-93.

New Model-Free Daily Inversion of NO_x Emissions using TROPOMI (MCMFE-NO_x): Deducing a See-Saw of Halved Well Regulated Sources and Doubled New Sources

Kai Qin[1†], Jincheng Shi[1], He Qin[1], Weizhi Deng[2,3], Shuo Wang[4], Jian Liu[2], Jason B. Cohen[1*†]

[1]Jiangsu Key Laboratory of Coal-Based Greenhouse Gas Control and Utilization, School of Environment and Spatial Informatics, China University of Mining and Technology, Xuzhou

[2]Department of Atmospheric Sciences, Sun Yat-Sen University, Zhuhai

[3]Now at: Department of Chemical & Biochemical Engineering, The University of Iowa, Iowa City, IA, USA

[4]College of Meteorological Observation, Chengdu University of Information Technology, Chengdu

[*]Correspondence to jasonbc@alum.mit.edu / jasonbc@cumt.edu.cn

[†]These authors contributed equally to this work

Abstract

Current approaches to estimate NO_x emissions fail to account for new and small sources, biomass burning, and sources which change rapidly in time, generally don't account for measurement error, and are either based on models, or do not consider wind, chemistry, and dynamical effects. This work introduces a new, model-free analytical environment that assimilates daily TROPOMI NO_2 measurements in a mass-conserving manner, to invert daily NO_x emissions. This is applied over a rapidly developing and energy-consuming region of Northwest China, specifically chosen due to substantial economic and population changes, new environmental policies, large use of coal, and access to independent emissions measurements for validation, making this region representative of many rapidly developing regions found across the Global South. This technique computes a net NO_x emissions gain of 70% distributed in a see-saw manner: a more than doubling of emissions in cleaner regions, chemical plants, and regions thought to be emissions-free, combined with a more than halving of emissions in city centers and at well-regulated steel and powerplants. The results allow attribution of sources, with major contributing factors computed to be increased combustion temperature, atmospheric transport, and in-situ chemical processing. It is hoped that these findings will drive a new look at emissions estimation and how it is related to remotely sensed measurements and associated uncertainties, especially applied to rapidly developing regions. This is especially important for understanding the loadings and impacts of short-lived climate forcers, and provides a bridge between remotely sensed data, measurement error, and models, while allowing for further improvement of identification of new, small, and rapidly changing sources.

1. Introduction – Background

Oxides of Nitrogen (NO_x) are associated with high temperature combustion in the atmosphere, and are directly produced by fossil fuel combustion, fires, biomass burning, industry, shipping, electric discharge, and other sources (Brewer et al., 1973; Logan 1983). NO_x is one of the set of short-lived trace gasses which are considered short-lived climate forcers (SLCFs), with direct impacts on: human health, nitrate aerosol (an important component of scattering aerosols) and tropospheric ozone (which is both air pollutant and greenhouse gas) (Chen et al., 2007; Collins et al., 2013; Crutzen, 1970; Jacob et al., 1996; Li et al., 2018; Monks et al., 2015; Rollins et al., 2012; Sand et al., 2016; Seinfeld, 1989; Shindell et al., 2012; Tan et al., 2018). Presently, there are techniques to observe the local surface concentration of NO_x and the remotely sensed total column of NO_2 from both surface and satellite platforms. However, due to rapid chemical reactivity, non-linear interactions with UV radiation and VOCs, sensitivity to combustion temperature, and rapid chemical change between NO_2 and NO, there is no simple way to approximate emissions of NO_x at high spatial and temporal resolution (Alvarado et al., 2010; Lueue et al, 2001; Martin et al., 2003; Martin et al., 2006; Mijling et al., 2013).

Present methods to approximate SLCF emissions lead to results which tend to underestimate actual emissions in those regions of the world which are rapidly developing (Cohen and Wang, 2014; Lei et al., 2014; Lin et al., 2020; Wang et al., 2021). The first general method is based on sets of equations referred to as bottom-up aggregation, in which small geographic and temporal scale measurements made in the laboratory or field are aggregated together with economic and technological data (Li et al., 2017; Oliver et al., 1994; van Amstel et al., 1999). The second approach uses directly measured point-source measurements such as those made via local flux towers (Geddes and Murphy, 2014; Haszpra et al., 2018; Karl et al., 2017; Lee et al., 2015). The third approach uses chemical transport models and either a Bayesian, 3D/4D variance, or Kalman Filter type of inversion (Cohen and Wang, 2014; Henderson et al., 2012; Hu et al., 2022; Napelenok et al., 2008). A final approach is limited to special situations where there is a single very strong, non-time varying source surrounded by relatively clean upwind regions, coupled with Gaussian plume modeling (Beirle et al., 2011; Beirle et al., 2019; Cohen and Prinn, 2011; de Foy et al., 2014; Jin et al., 2021; Laughner and Cohen, 2019), or by taking the data over a long period of time during a specific season of the year and approximating a general emissions estimation, and assuming it is uniform over the averaged spatial and/or temporal domain (Kong et al., 2022). Due to the approximations associated with each method, there are some constant problems: underapproximation or complete miss of small and moderate sources (Drysdale et al., 2022); underestimation of sources with a large amount of temporal and spatial variability (Cohen, 2014; Stavrakou et al., 2016; Vaughan et al., 2016; Wang et al., 2010; Zyrichidou et al., 2015); and over-dependence on a priori estimates (Zhao and

Wang, 2009). Furthermore, other than the computationally expensive Kalman Filter approach, these methods do not provide robust uncertainly analysis (Cohen and Wang, 2014; Lin et al., 2020; Wang et al., 2021a). At the present time, emissions used to drive the loading and distribution of both aerosols and ozone in climate models rely heavily on static bottom-up approaches (Oliver et al., 1994; van Amstel et al., 1999). This has limited nearly all perturbation studies of SLCF to merely scaling up and down existing distributions in space and time to attempt to look for a scaled perturbation signal, and then averaging the resulting signal, effectively ignoring significant variations in space and time, such as wildfires and new urbanization, which are both expected to increase in magnitude in the future as the climate continues to change (Deng et al., 2021; Evangeliou et al., 2018; Lund et al., 2020).

This work introduces a new approach to compute NO_x emissions, using a mass conserving model free approximation [MCMFE-NO_x] based on daily remotely sensed column measurements of NO_2 from TROPOMI at $0.05^o \times 0.05^o$ spatial resolution, reanalysis 3-hourly wind fields, and a 4-term mass conservation approximation. This technique permits a robust quantification of the underlying thermodynamics driving the ratio of the primary emissions NO_x to NO_2, both advective and pressure-induced dynamical transport, and a first order approximation of the underlying in-situ chemical loss of NO_x. The computed uncertainty associated with each individual underlying factor as well as the remotely sensed measurements is quantified. The resulting fits allow a rapid check to determine if the underlying driving terms are consistent with known physical, chemical, and thermodynamic principles, allowing for climate-induced feedbacks on emissions to be integrated into climate runs. Since no complex modeling is required, MCMFE-NO_x is readily accessible to use in connection with the current batch of climate models, without added additional computational costs (Cohen and Prinn, 2011; Cohen et al., 2011; Holmes et al., 2013; Prinn, 2013).

MCMFE-NO_x is applied using one year of daily TROPOMI NO_2 observations over the newly developing, energy-rich, triangular-shaped region of Northwestern China called the "Golden Energy Triangle" (Chen et al., 2010; Liang et al., 2019; Ling et al., 2017; Shen et al., 2016), consisting of Ningxia, and parts of Shaanxi, Inner Mongolia, and Shanxi Provinces. This region is a large producer and consumer of coal for local power generation, export of power to commercial and highly developed regions in Eastern China (such as Jiangsu and Shanghai), steel, chemicals, materials, heavy industries, and energy-intensive desert agriculture, among other uses (Chen et al., 2010). This region consists of well-established chemical factories and urban areas in Yinchuan and Yulin, power production in Wuhai, and steel mills and urbanization in Baotou, in addition to new and rapidly expanding urban areas (Huhehaote and Eerdousi), coal-fired power production (around Wuhai), steel production (around Baotou), and chemical industry (Xiaoyi and expansion around both Yinchuan and Yulin). Due to its rapidly growing economy and large population change, there is expected to be a significant change in emissions over the last decade (Stavrakou et al., 2008; Streets and Waldhoff, 2000) as demonstrated in a set of recently taken

photographs of the coal-fired power plants and chemistry plants in Ningdong and steel factories in Baotou (Figure 1). This area is well representative of the types of new industry and economic growth occurring throughout the Global South, and any biases found in the emissions from this region are likely to also be found in other rapidly developing and energy intensive regions around the world (Rogelj et al., 2014).

It is essential that emissions used to drive global and regional climate models are consistent with actual emissions to the atmosphere at high temporal and spatial resolution in order to simulate the impacts of short-lived climate forcers (Aamaas et al., 2017; Zheng and Unger, 2021). The results presented here are successful at capturing existing and growing urban areas, coal-fired power plants, chemical plants, iron and steel production, and other industrial sources, while further providing insight into what controls these sources. The impacts of changes in urban, industrial, and transportation sources associated with a growing middle class are observed, with the results comparing excellently with an independent set of measurements of small to medium industrial sources, especially so at over geographic areas in which there is no a priori emissions estimate, indicating the growing importance of moderate and small emissions sources (van der A et al., 2020; Wang et al., 2012). Furthermore, the variability in the emissions estimates demonstrate clear impacts of meteorology, photochemistry, emissions thermodynamics, and terrain induced effects on NO_x emissions (Lin et al., 2021; Stavrakou et al., 2013; Tong et al., 2022). MCMFE-NO_x allows a consistent analysis of the natural and anthropogenic sources and in-situ evolution of NO_x emissions, and provides maps of when, where, and how to target emission controls in close-to real time. These are necessary steps for creating the next generation of emissions products which can be used to better understand the impacts of changes in the emissions of short-lived climate forcers, as well as to help better manage mitigation efforts to address these sources.

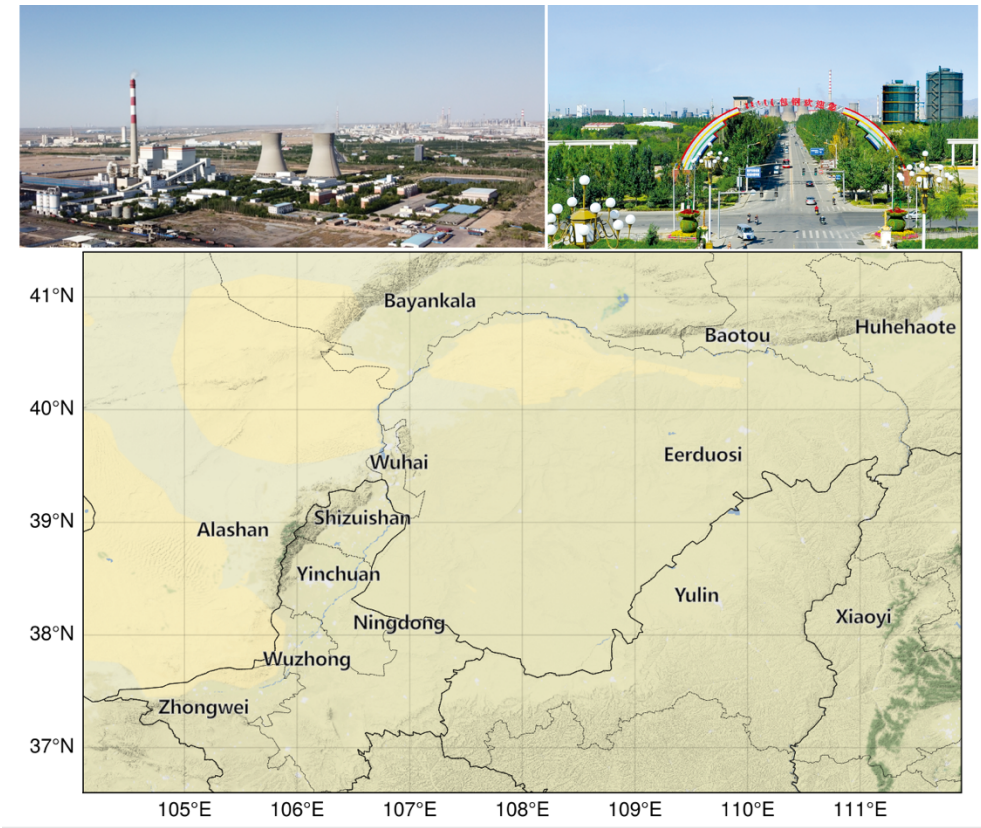

Figure 1: Recent photographs taken at Ningdong demonstrating a power plant and chemicals plant (top left), and Baotao demonstrating a steel plant (top right). A map of the region in this work, including all cities mentioned in the paper is given below.

2. Methods

2.1 Experimental Design

A graphical overview of the steps used in this work is provided in Figure 2. First, the VCDs from TROPOMI are quality controlled. Next, on a grid-by-grid, and day-by-day basis, the subset of pixels which contain valid VCDs are used in connection with a gold-standard a priori emissions database to make a monthly mass-conserving fit. These fitted values are then applied to all data, day-by-day and grid-by-grid where there is sufficient TROPOMI data, to produce emissions. In those grids which do not have best fit coefficients, a bootstrap approach is used.

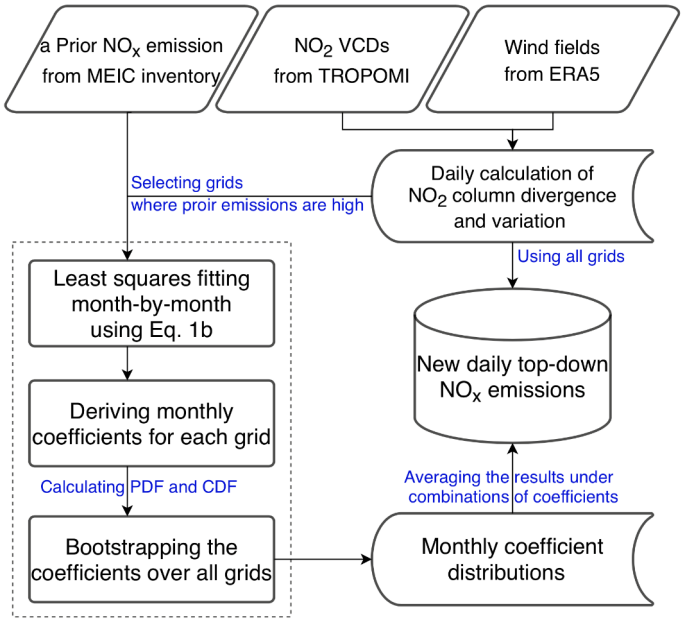

Figure 2. Flowchart describing the steps used to first develop MCMFE-NO_x.

2.2 Remotely Sensed Data

The TROPOMI spectrometer (Van Geffen et al., 2020; Veefkind et al., 2012) onboard Sentinel-5 Precursor (2017–today) has a local equator crossing time around 13:30 providing global afternoon coverage. TROPOMI measures backscattered solar UV, allowing the retrieval of the tropospheric NO_2 Vertical Column Densities (VCDs) with spatial resolution of 3.5kmx7km (3.5kmx5.5km since August 2019) at nadir. This work uses KNMI offline version 1.2/1.3 from 1 January 2019 to 31 December 2019, and further filters pixels with a qa_value <0.75. The overlapping NO_2 VCDs pixels in each swath are resampled to the common latitude-longitude grids with a size of 0.05°x0.05° using the weighted polygon shaped remotely sensed measurement toolkit HARP (http://stcorp.github.io/harp/doc/html/index.html).

There are natural factors which make this region an ideal case study for this new emissions estimation approach. The region has low cloud coverage, allowing for a higher density of remotely sensed TROPOMI measurements and higher measurement precision due to a lower level of cloud contamination (Liu et al., 2020; Platz et al., 1998). The vast majority of significant NO_x sources are separated by relatively empty land, and are of a size that they can be captured within a few grids, allowing for less complexity in terms of background effects and separation of upwind versus local sources (Cohen and Prinn, 2011). Furthermore, the climate, elevation and overall surface UV flux are somewhat similar throughout the region, indicating that chemical decay on average does not change too much.

Given the uncertainty of the NO_2 measurements is approximately $1.0x10^{15}$+30% molecules/cm^2 (computed as $1.4x10^{15}$ molecules/cm^2) therefore it is important to filter any data in which the annual mean of the data is smaller than this value, so as to not estimate emissions in regions in which the only basis is potential noise (Zhang and Schreifels, 2011). Furthermore, since at most points there is a considerable amount of missing data, to be certain that the data is reliable on a month-to-month basis, the mean value when taken over all days of the month (including missing data points) must also have a mean larger than $1.4x10^{15}$ molecules/cm^2. In all cases, these values are set to NaN and subsequently are not computed further.

2.3 Emissions a priori

The Multi-resolution Emission Inventory for China (MEIC) model provides a high-resolution bottom-up emission inventory of anthropogenic air pollutants over mainland China. NO_x emissions are provided on a total monthly basis across five sectors: agriculture, industry, power, residential and transportation. This work uses emissions from MEIC at a spatial resolution of 0.1°x0.1° and a temporal resolution of monthly, corresponding to 2015, as the a prior for the mass-conserving model employed herein, which is the latest emissions inventory available China-wide. To be consistent with the other units, the monthly NO_x emissions are assumed constant day-to-day and therefore are converted to $ug/m^{-2}s^{-1}$, and this value is used as the a prior for each month. This resulting output is interpolated to the TROPOMI spatial resolution by the nearest neighbor method. For this study, we discarded the bottom 2.5 percentile of emissions, so as to ensure that the values used are not within the error range of the TROPOMI measurements. Furthermore, to ensure representativeness between the a priori data the results, especially due to the increased UV radiation and hence chemical reactivity at height, since there is no a priori emissions data available at elevations greater than 1500m, all data above this height are also set to NaN and subsequently are not computed further.

2.4 China EPA Powerplant Emissions Data

The continuous emissions monitoring system (CEMS) was introduced by the ministry of environmental protection of China (MEP) in 2007 to monitor and manage the emissions of state-controlled key coal-fired power plants and large industrial boilers (Tang et al., 2020). CEMS is designed to provide direct, real-time, continuous measurements of pollutant concentrations and air flow through the stack into the atmosphere, from coal-fired power plants, steel plants, cement plants, boilers and so on (Karplus et al., 2018; Tang et al., 2020). Each CEMS is required to provide real-time data feeds to the automatic monitoring and control system in national, provincial and municipal environmental protection agencies (Tang et al., 2020). The CEMS data used in this work was collected from the Energy Big Data network, and provides monthly data for 2017 and 2019 (http://energy.ckcest.cn/index).

2.5 Statistical Methods

Daily data from TROPOMI and the ECMWF reanalysis is grouped month-by-month at each 0.05°x0.05° spatial-grid together with the best-of-class monthly a priori emissions dataset for China using MEIC to compute the best fitting value for $_1$, $_2$, and $_3$ grid-by-grid, month-by-month using a multiple least squares regression (MLR) fitting approach. To compute both the best 4computed, data is required both on the day of interest itself, as well as the day before, the day after, and each of the adjacent 4 grids on the day being analyzed. The horizontal gradients are specifically computed in both the x and y directions using data from four adjacent boxes on the same day as the measurement. The temporal gradients are computed using both the value from the past day, the present day, and the future day on the same grid as being computed. In terms of fitting the values of $_1$, $_2$, and $_3$, best fits were made using MLR month-by-month and pixel-by-pixel. This approach is valid when there are at least 4 data points available for each fit of the three respective terms. For pixels in specific months that do not have enough data to make a successful fit, or a p value larger than 0.05, the values of $_1$, $_2$, and $_3$ are set to nan.

By solving the terms month-to-month, the resulting approximations are more able to reproduce the different chemical and transport forcings observed during different times of the year. Monthly aggregated PDFs for each of $_1$, $_2$, and $_3$ are provided respectively as figures S1-ii, S2-ii, and S3-ii at https://www.doi.org/10.6084/m9.figshare.19560517 where ii is the month, while the climatological mean values of $_1$, $_2$, and $_3$ are given in Figure 3. There is a moderate amount of variation observed between the resulting PDFs in different months, with the largest differences observed between August (most variable distributions of $_1$, $_2$, and $_3$) and January (least variable distributions of $_1$, $_2$, and $_3$).

Since some of the MLR fits may occasionally lead to extreme values of $_1$, $_2$, and $_3$ which are not physically realistic, it is essential to find a reasonable range of coefficients to use to predict the emissions. To this aim, a bootstrap approach is used to estimate the maximum probability density of the three coefficients on a month-by-month basis. The bootstrap was done using a sampling frequency of 3000, and a confidence level of 95%. The corresponding coefficient confidence interval was obtained and compared against reasonable limits imposed by both the underlying chemistry and physics. All non-realistic terms (such as positive chemical decay rates, unreasonably fast or slow for chemistry, and ratios of NO_x/NO2 which are too small to exist in the real atmosphere) were set to nan. Furthermore, these conditions were not observed to exist in any of the post bootstrap outputs.

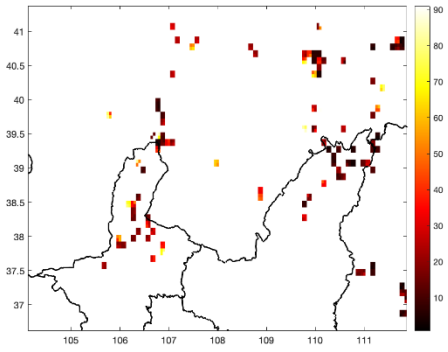
41
40.5
40
39.5
39
38.5
38
37.5
37
105
106
107
108
109
110
111
90
80
70
60
50
40
30
20
10

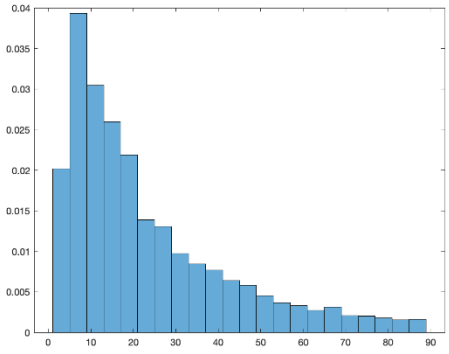
0.04
0.035
0.03
0.025
0.02
0.015
0.01
0.005
0
0
10
20
30
40
50
60
70
80
90

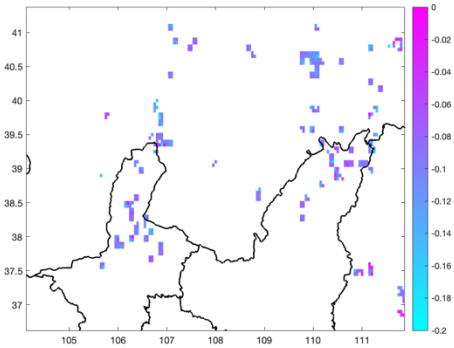
41
40.5
40
39.5
39
38.5
38
37.5
37
105
106
107
108
109
110
111
0
-0.02
-0.04
-0.06
-0.08
-0.1
-0.12
-0.14
-0.16
-0.18
-0.2

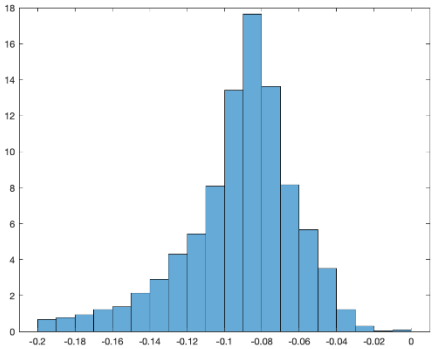
18
16
14
12
10
8
6
4
2
0
-0.2
-0.18
-0.16
-0.14
-0.12
-0.1
-0.08
-0.06
-0.04
-0.02
0

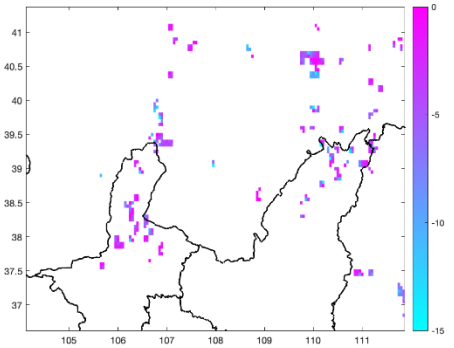
41
40.5
40
39.5
39
38.5
38
37.5
37
105
106
107
108
109
110
111
0
-5
-10
-15

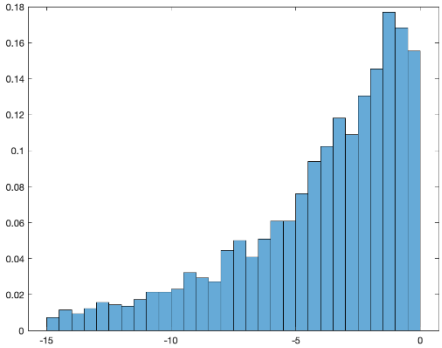
0.18
0.16
0.14
0.12
0.1
0.08
0.06
0.04
0.02
0
-15
-10
-5
0

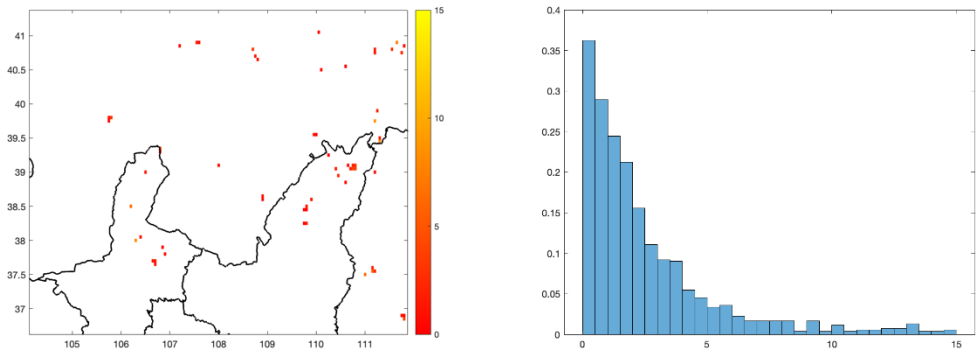

Figure 3: Computed values of: (top row) climatological map and month-by-month PDF of $_1$ [NO_x/NO_2]; (second row) climatological map and month-by-month PDF of $_2$ [days]; (third row) climatological map and month-by-month PDF of $_3$ out from sources [km]; and (fourth row) climatological map and month-by-month PDF of $_3$ in to sources [km].

When the values of $_1$, $_2$, and $_3$ are used to compute the emissions, first statistical samples of $_1$, $_2$, and $_3$ are repeated 1000 times using a bootstrap approach based on a random sampling from each respective PDF, within the ranges given in Figure 3. The equations are integrated using the TROPOMI NO_2 columns, a priori emissions, and meteorology such that it is temporally and spatially consistent, using all days of data available where data exists on the day being computed, either the day before or after (for the time gradient), on the same day being computed at least one surrounding grid (for the horizontal gradient), and in combination with the sampled values of $_1$, $_2$, and $_3$ having an available best fit value during the respective month. For grids with data and with a set of $_1$, $_2$, and $_3$ the bootstrap approach is used, while for grids with existing $_1$, $_2$, and $_3$ only these values are used.

3. Results

The 2019 annual mean of daily NO_2 column loading and its probability distribution function [PDF], and the annual standard deviation of daily NO_2 columns (post-filtered for signals smaller than the measurement uncertainty) and its PDF are mapped in (Figure 4), provide a quantitative measure of the signal's climatology and variability (Cohen, 2014; Lin et al., 2020; Stavrakou et al., 2016; Verhoelst et al., 2021). High average values with a relatively low normalized standard deviation are observed in known urban and coal consuming areas, consistent with well characterized and regulated sources (Lin et al., 2020). Data with a moderately high NO_2 column and moderately high normalized standard deviation are observed in suburban areas as well as in some outlying areas far from existing energy, steel, and chemical factories, including in locations completely removed from substantial or village level administrative regions (Deng et al., 2021). Such combination of mean and standard deviation has been pre-

viously observed in biomass burning regions, which are not prevalent in the region of this study, and therefore likely indicate an anthropogenic source undergoing rapid change or otherwise mis-identified or mis-characterized (Wang et al., 2021a).

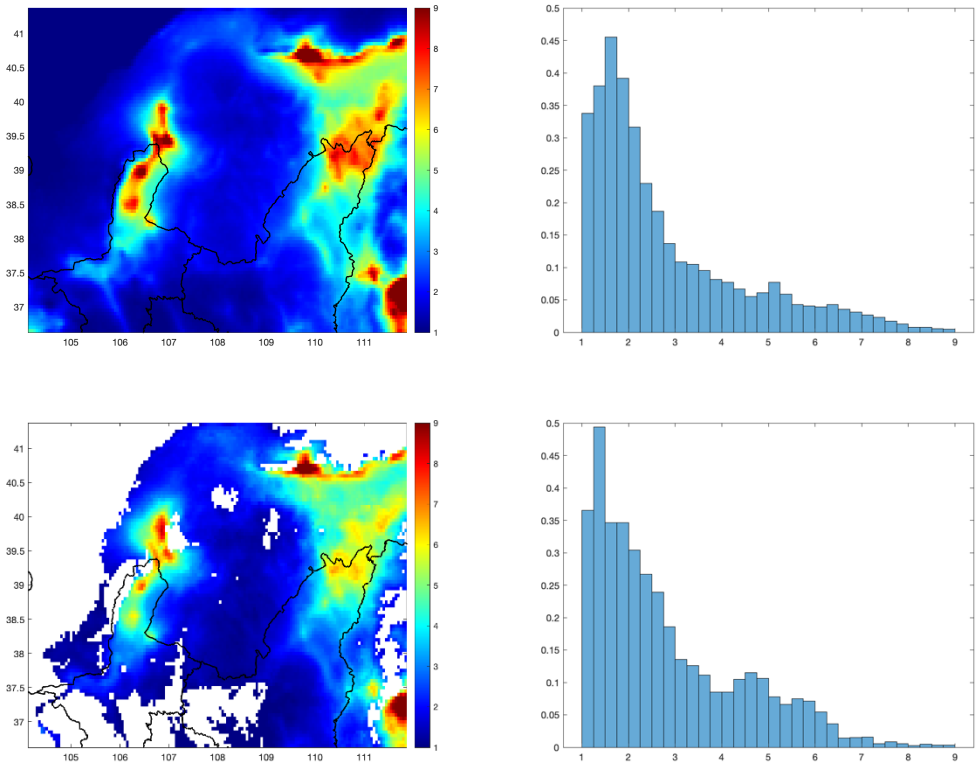

Figure 4: TROPOMI daily average climatological NO_2 column loading [10^{15} molec/cm^2]: (top left) mean, (top right) PDF of mean, (bottom left) standard deviation, and (bottom right) PDF of standard deviation.

The mass conservation equation for NO_x in-situ is a function of column NO_2 measurements via the linear transformation $NO_x = {}_1NO_2$, consistent with the fact that after emission, the ratio of NO_2 to NO_x achieves a rapid local pseudo-steady state equilibrium (Mavroidis and Chaloulakou, 2011) and that NO isn't readily measurable via remote sensing. This assumption has been adapted as a fixed value by the emissions and chemical modeling communities with a range of values from 9 to 19 (Oliver et al., 1994; van Amstel et al., 1999), while in this work, the value of ${}_1$ is allowed to vary based on the best fit between the measurements, meteorology, and the a priori emissions data, allowing for an optimal range of values that is still thermodynamically realistic (Chong et al., 2010). Post-transformation, mass conservation equation is based on measure-

ments of NO_2, as given in Equation 1a. Equation 1a is rearranged to Equation 1b to solve for the emissions of NO_x [E_{NOx}], where $_2$ represents chemical decay of NO_x and $_3$ represents the advective and pressure transport of NO_x.

$$d(\ _1[NO_2])/dt = E_{NOx} + \ _2(\ _1[NO_2]) + \ _3\ (u\ _1[NO_2]) \quad (1a)$$

$$E_{NOx} = \ _1d([NO_2])/dt - \ _2\ _1[NO_2] - \ _3\ _1\ (u[NO_2]) \quad (1b)$$

3.1 Emissions Drivers

The terms completely govern the mass-balance of NO_x: (a) the scaled change in measured NO_2 between the previous day's and present day's measurements, (b) the present day's a priori emissions [for fitting] or computed MCMFE-NO_x [prediction], (c) the scaled change in the present day's measurement due to chemical decay, (d) the scaled change in the present day's measurement due to horizontal advection in or out of the geographic location, and (e) the scaled change in the present day's measurement due to the squeezing or thinning of air at the geographic location. The final assumption is that NO_x emissions are roughly uniform throughout the day, allowing the integrated net effect of those processes with an effect faster than the one-day time step to be representative throughout the day, a reasonable assumption on the scales being analyzed in this work (Cohen and Prinn, 2011; He et al., 2020).

PDFs of the best fit values of $_1$, $_2$, and $_3$ (Figure 3) are constrained by idealized and field measurements, allowing for greater variability than many current models provide, while still being consistent with real world conditions (Laughner and Cohen, 2019). The 30%, median, and 70% values of $_1$ are 9.6, 16.9, and 29.2 respectively, covering the range used by community models, but with a wider range on the high side (less NO_2 in NO_x), consistent with higher temperature combustion associated with ever-increasing energy efficiency of coal boilers (Cox, 1999; van Der A et al., 2008). The 30%, median, and 70% values of $_2$ are -0.076days, -0.089days, and -0.11days respectively, covering the range of values in community models, but with a wider range on the negative side (faster chemical reactivity) consistent with theory and measurements in other similar geographic regions, which are both at higher elevation and which tend to be relatively cloud free (Beirle et al., 2011; Laughner and Cohen, 2019). The 72% of cases in which the transport is negative (net export) have a 30%, median, and 70% values of $_3$ of -1.8km, -3.5km, and -6.0km respectively, while the 28% of cases in which transport is positive (net import) have a 30%, median, and 70% values of $_3/\ _1$ of 0.9km, 1.7km, and 3.2km. These values include values of fluxes advected into source emitting regions, something that current models do not represent well but is known to exist from observations, as well as slightly smaller than current modeled transport exported from emitting regions into remote downwind regions (Aouizerats et al., 2015; Cohen et al., 2011; Lee et al., 2017).

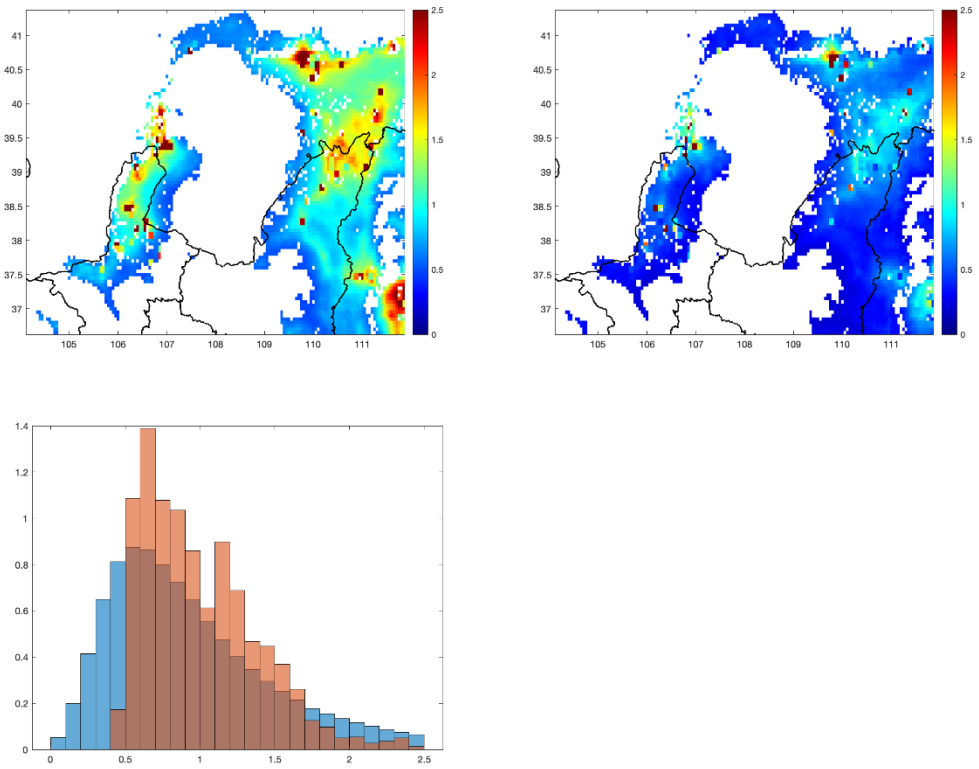

Figure 5: Representations of daily computed MCMFE-NO_x [µg/m^2s]: (a) climatological mean, (b) climatological standard deviation, and (c) histograms of all daily data (blue), and of the grid-by-grid climatological mean data (red).

3.2 Emissions See-Saw

Equation 1b is solved daily by sampling from the respective monthly PDFs of $_1$, $_2$, and $_3$, TROPOMI NO_2 and reanalysis wind. The annual mean and standard deviation of the daily emissions are given in (Figure 5) with the day-to-day results available for download at https://www.doi.org/10.6084/m9.figshare.19560517. Emissions cover 35% of the spatial domain, with an average daily value of 1.1±1.0µg/m^2s, as compared with the a priori which covers 14% of the domain and has a mean value of 0.78±1.7µg/m^2s.

The majority of the increase in emissions occurs in grids with low a priori emissions (hereafter defined as <1.1µg/m^2s), with MCMFE-NO_x computed to be 1.2±0.44µg/m^2s compared to the a priori emissions of 0.22±0.26µg/m^2s, consistent with new and increasing small and moderate sources (Figure 6). Oppositely, on those grids with a high a priori emissions (hereafter defined as >1.1µg/m^2s), MCMFE-NO_x are found to be slightly lower at 2.7±2.4µg/m^2s compared to the a priori emissions 3.0±2.7µg/m^2s, consistent with a slow but continuous reduc-

tion in emissions from known and well-regulated sources such as urban centers and large steel, chemical and power plants. These findings are consistent with recent laws in China targeting controls at well-known sites to bring them under stricter compliance.

MCMFE-NO_x over grids without a priori data (newly identified sources) has a low value of $0.95 \pm 0.42 \mu g/m^2 s$ and covers 27% of the domain. Conversely, grids which contain a priori emissions without MCMFE-NO_x (well-controlled sources) yield a result with a low average and high variance value of $0.68 \pm 1.6 \mu g/m^2 s$ and cover 14% of the domain, demonstrating a large amount of variability. Thus, heavily polluting sites have emissions consistent with increasing energy efficiency, successfully abated or mitigated NO_x sources, and/or have been possibly shut down, while at the same time a large number of small and medium emitting sites are more active than before, new, or were previously mis-identified.

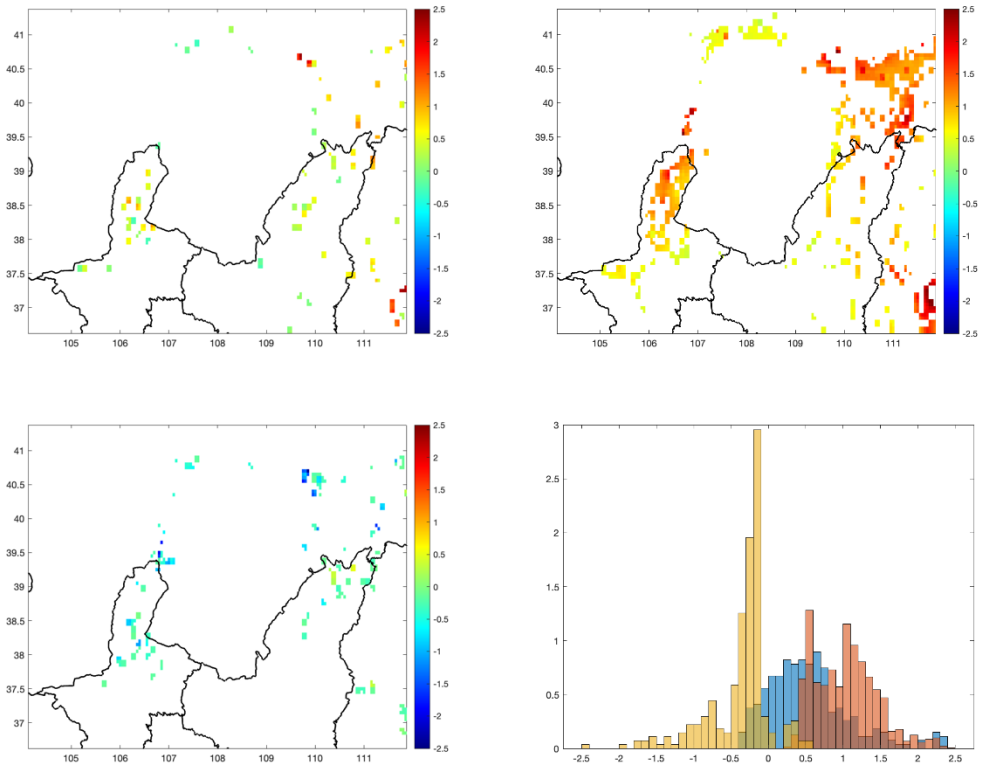

Figure 6: Difference between MCMFE-NO_x [$\mu g/m^2 s$] and: (a) MEIC (when between $0.3 \mu g/m^2 s$ and $1.1 \mu g/m^2 s$), (b) MEIC (when less than $0.3 \mu g/m^2 s$), and (c) MEIC (when larger than $1.1 \mu g/m^2 s$). (d) PDFs of cases (a) blue, (b) red, and (c) orange.

Integrating over the domain MCMFE-NO_x is 1.90Mton/yr, compared with the

a priori net emissions of 1.10Mton/yr. MCMFE-NO_x in newly identified areas is 1.18Mton/yr, and MCMFE-NO_x in grids with a low a priori is 0.47Mton/yr, compared with the a priori total over low regions of 0.26Mton/yr. MCMFE-NO_x in highly emitting areas including urban centers, major coal fired power plants, chemistry plants, and steel plants is 0.24Mton/yr, compared to the a priori emissions of 0.85Mton/yr.

3.3 Comparison with EPA Emissions

On the 56 grids which have emissions computed using an independent stack-based concentration measurement approach at power plants, steel plants, and coal to chemicals plants [CEMS] that overlap with MCMFE-NO_x grids, the average emissions are 2.1±2.1μg/m^2s and 1.2±0.98μg/m^2s respectively (Figure 7). The match is closer between the 25 MCMFE-NO_x grids which do not contain a priori emissions 1.1±0.38μg/m^2s and CEMS 1.1±0.58μg/m^2s, than between the 12 grids at which all of MCMFE-NO_x 1.3±0.41μg/m^2s, CEMS 1.0±0.48μg/m^2s, and the a priori emissions 0.43±0.28μg/m^2s all overlap. On the 51 grids where a priori emissions overlap with CEMS, the a priori emissions 2.7±3.0μg/m^2s has less overlap with CEMS 1.0±1.1μg/m^2s than the 56 grid overlap between CEMS and MCMFE-NO_x. Furthermore, the 11 grids where a priori emissions overlap with CEMS and do not have any MCMFE-NO_x data, the difference between the a priori 3.5±3.0μg/m^2s and CEMS 1.0±0.71μg/m^2s is larger still. These results clearly demonstrate that MCMFE-NO_x has a closer fit to and less bias with respect to CEMS than the a priori.

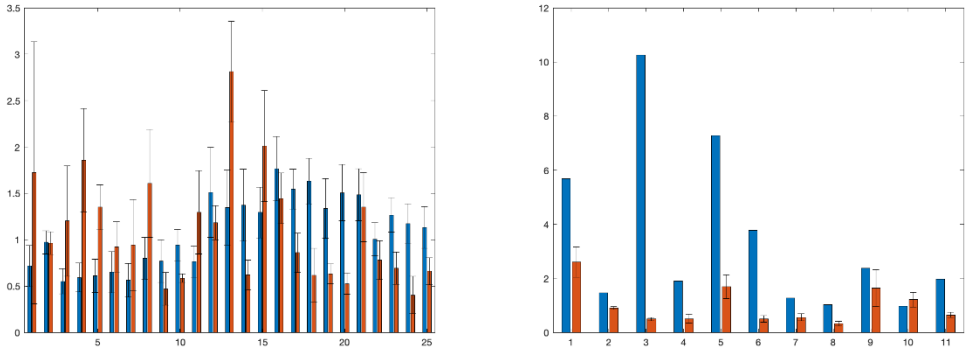

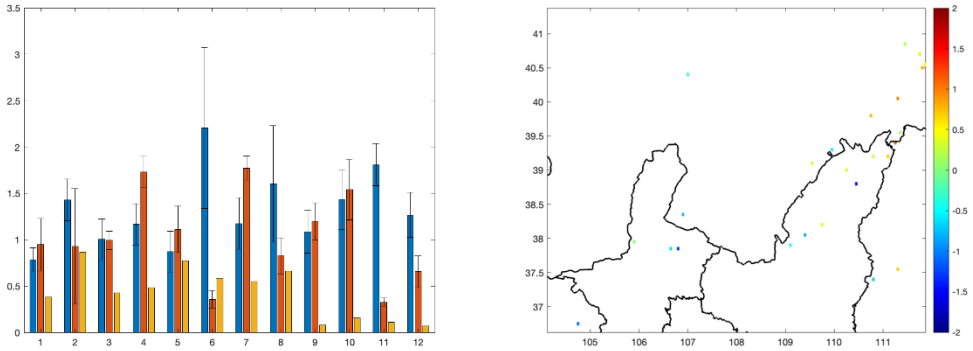

Figure 7: Comparison of annual emissions (bars) and 1 standard deviation uncertainty ranges (lines) for the following cases: (a) 25 sites which overlap between MCMFE-NO_x (blue) and CEMS (red), (b) 11 sites which overlap between the a priori (blue) and CEMS (red), and (c) 12 sites which overlap between MCMFE-NO_x (blue), CEMS (red), and the a priori (orange). (d) Map of the difference in emissions given in (a).

4. Discussion

The emissions computed using daily NO_2 measurements and the 4-term mass conservation approach are 1.7 times higher than emissions from the gold-standard bottom-up inventory. However, there is a clear difference in geography and two contributing factors. First, emissions in known urban centers and large coal consuming areas (Yinchuan, Baotao, Wuhai, and Yulin) are 28% of the a priori value. Second, emissions in regions with a low a priori or no a priori emissions, specifically with new or growing chemical industries (Xiaoyi and expansion around Yinchuan and Yulin), new coal-based powerplants (expansion around Wuhai), new steel production (expansion outside of and around Baotou), and regions with new or significantly expanding urban cores (Huhehaote and Eredosi) have a computed emissions 250% the a priori value. This see-saw of increasing emissions in rapidly changing areas combined with decreasing emissions in more established, closely monitored, and more regulated regions, is consistent with the rapid economic development, population shifts, and policies implemented. Furthermore, the emissions match better with independent stack-based measurements of emissions, overall, as well as in terms of the conclusions above: the lower emitting stacks tend to have a slightly higher total emissions from MCMFE-NO_x, consistent with other sources associated with the activity present at the stack sites, while the higher emitting stacks tend to have a lower total emissions from MCMFE-NO_x, still larger than the stack values themselves, but only barely, again consistent with increased regulation. MCMFE-NO_x also identifies new sources including new or growing small-scale industry, biomass and agricultural burning, and residential sources, and in particular fits the stack-based emissions much better

in regions without a priori emissions.

4.1 Gleaning Information about Combustion, Chemistry, and Transport

There is a significant number of grids which are have an emissions ratio of NO_x/NO_2 outside of the range used in chemical transport models, yet still consistent with thermodynamics and observation studies, indicating that this result accounts for more real-world variability (Mavroidis and Chaloulakou, 2011; Oliver et al., 1994; van Amstel et al., 1999). The large value of $_1$ around Wuhai and Baotou is consistent with increased NO occurring at higher temperature combustion conditions, consistent with the increased energy efficiency of thermal power plants and steel production sites. The small value of $_1$ in Xiaoyi, Yinchuan, and Ningdong is consistent with less efficient and lower temperature combustion conditions associated with coal to chemical plants, residential, and transportation sources. The generally more negative values of $_2$ are consistent with faster chemistry than currently used in the modeling community (Laughner and Cohen, 2019), but are consistent with observations in regions with higher amounts of surface UV irradiance, consistent with the geography of the region studied here (Cadet et al., 2020). The magnitude of $_3$ is observed to provide a significant amount of NO_x transport over 44 continuous grids around Baotou and 22 continuous grids around Wuhai, in contrast to most studies indicating little long-range transport. The results are consistent with proximity to mountains being one major driving factor (Bonasoni et al., 2010). Interestingly $_3$ has a positive value over 5 continuous grids in Eerduosi, indicating transport does contribute to NO_x in some urban areas, a significant break with traditional assumptions that boundary layer height, local emissions, and wind speed control sources in urban centers, but consistent with idealized studies (Cohen and Prinn, 2011; Cohen et al., 2011). Hence MCMFE-NO_x can quantify the contributions on NO_x emissions and loadings based on source thermodynamics and efficiency, chemical and radiative conditions, atmospheric properties, measurement uncertainty, and even topography.

4.2 Limitations and Applications

There are at least three limitations in this work. The remotely sensed dataset analyzed in this work has daily data over 1 year at a spatial resolution of 3.5km×7/5.5km, meaning studies requiring higher resolution or similar resolution at longer time-scales cannot be made. Secondly, the region analyzed is relatively homogenous in terms of sources, geography, and a priori emissions, and therefore this approach may not work well in a region which is more heterogenous in terms of emissions sources, geographic conditions, and other phenomena impacting the remotely sensed retrievals. Furthermore, the chemical decay and transport are both limited to first-order processes, which may not work well under highly polluted conditions, or in the case of a large number of individual sources in close geographic proximity, requiring further enhancements to the mass-conserving equations in these regions to better account for non -linear effects.

Applications focusing on expanding the procedure to other rapidly changing source regions, extending the analysis over longer period of time, and using a greater number of a priori emissions sources would all be logical next steps. Expanding the values obtained to other global regions which are climatologically and technologically similar but located in different regions of the world would also make for impactful follow-up. Furthermore, expanding into regions with few or no a priori emissions inventories could add further value. Additionally, analysis using smarter sampling and fitting could also lead to an increase in the robustness of the solution. On top of this, working iteratively with the bottom-up emissions community to adapt these emissions datasets, and then using the enhanced a priori datasets to re-drive this process could provide tighter uncertainty bounds and reduce biases. Finally, this method could be used by the air pollution control community to rapidly identify and/or predict specific extreme air pollution events.

Description of author's responsibilities

This work was conceptualized by Jason Blake Cohen and Kai Qin. The methods were developed by Jason Blake Cohen and Kai Qin. Investigation was done by Jincheng Shi, Kai Qin, and Jason Blake Cohen. Visualizations were made by He Qin, Jincheng Shi, and Jason Blake Cohen. Writing of the original draft was done by Kai Qin, Jason Blake Cohen, Jincheng Shi, He Qin, Shuo Wang, Jian Liu, and Weizhi Deng. Writing at the review and editing stages were done by Kai Qin and Jason Blake Cohen.

Funding

This work was supported by the National Natural Science Foundation of China [Grant Numbers 42075147, 41975041]; Shanxi Province Major Science and Technique Program [Grant Number 202101090301013]; and the Major research project of Jiangsu Key Laboratory of Coal-based Greenhouse Gas Control and Utilization [Grant Number 2020ZDZZ03A].

Data Statement

All data presented in and underlying the figures, the daily gridded MCMFE-NO_x emissions, and the computed monthly gridded values of $_1$, $_2$, and $_3$ are free for download at: https://www.doi.org/10.6084/m9.figshare.19560517. The TROPOMI data used in this work is available for download at: https://sentinel.esa.int/documents/247904/ 2476257/Sentinel-5P-TROPOMI-ATBD-NO2-data-products.

References

Aamaas, B., Berntsen, T. K., Fuglestvedt, J. S., Shine, K. P., & Collins, W. J. (2017). Regional temperature change potentials for short-lived climate forcers

based on radiative forcing from multiple models, *Atmos. Chem. Phys.*, 17, 10795–10809.

Alvarado, M. J., Logan, J. A., Mao, J., Apel, E., Riemer, D., Blake, D., ... & Sager, P. L. (2010). Nitrogen oxides and PAN in plumes from boreal fires during ARCTAS-B and their impact on ozone: an integrated analysis of aircraft and satellite observations. *Atmospheric Chemistry and Physics*, *10*(20), 9739-9760.

Aouizerats, B., Van Der Werf, G. R., Balasubramanian, R., & Betha, R. (2015). Importance of transboundary transport of biomass burning emissions to regional air quality in Southeast Asia during a high fire event. *Atmospheric chemistry and Physics*, *15*(1), 363-373.

Beirle, S., Boersma, K. F., Platt, U., Lawrence, M. G., & Wagner, T. (2011). Megacity emissions and lifetimes of nitrogen oxides probed from space. *Science*, *333*(6050), 1737-1739.

Beirle, S., Borger, C., Dörner, S., Li, A., Hu, Z., Liu, F., ... & Wagner, T. (2019). Pinpointing nitrogen oxide emissions from space. *Science advances*, *5*(11), eaax9800.

Bonasoni, P., Laj, P., Marinoni, A., Sprenger, M., Angelini, F., Arduini, J., Bonafè, U., Calzolari, F., Colombo, T., Decesari, S., Di Biagio, C., di Sarra, A. G., Evangelisti, F., Duchi, R., Facchini, MC., Fuzzi, S., Gobbi, G. P., Maione, M., Panday, A., Roccato, F., Sellegri, K., Venzac, H., Verza, GP., Villani, P., Vuillermoz, E., and Cristofanelli, P. (2010) Atmospheric Brown Clouds in the Himalayas: first two years of continuous observations at the Nepal Climate Observatory-Pyramid (5079 m). *Atmos. Chem. Phys., 10*, 7515–7531.

Brewer, A. W., McElroy, C. T., & Kerr, J. B. (1973). Nitrogen dioxide concentrations in the atmosphere. *Nature*, *246*(5429), 129-133.

Cadet, J. M., Bencherif, H., Cadet, N., Lamy, K., Portafaix, T., Belus, M., Brogniez, C., Auriol, F., Metzger, J.M., & Wright, C.Y. (2020) Solar UV Radiation in the Tropics: Human Exposure at Reunion Island (21 degrees S, 55 degrees E) during Summer Outdoor Activities. *Int J Environ Res Public Health*, *17*(21), 8105.

Chen, T. M., Kuschner, W. G., Gokhale, J., & Shofer, S. (2007). Outdoor air pollution: nitrogen dioxide, sulfur dioxide, and carbon monoxide health effects. *The American journal of the medical sciences*, *333*(4), 249-256.

Chen, W., Li, H., & Wu, Z. (2010). Western China energy development and west to east energy transfer: Application of the Western China Sustainable Energy Development Model. *Energy Policy*, *38*(11), 7106-7120.

Chong, J. J., Tsolakis, A., Gill, S. S., Theinnoi, K., & Golunski, S. E. (2010). Enhancing the NO_2/NO_x ratio in compression ignition engines by hydrogen and reformate combustion, for improved aftertreatment performance. *International Journal of Hydrogen Energy*, *35*(16), 8723-8732.

Cohen, J. B. (2014) Quantifying the Occurrence and Magnitude of the Southeast Asian Fire Climatology. *Environmental Research Letters*, 9, 114018.

Cohen, J. B., & Prinn, R. G. (2011). Development of a fast, urban chemistry metamodel for inclusion in global models. *Atmospheric Chemistry and Physics*, *11*(15), 7629-7656.

Cohen, J. B., & Wang, C. (2014). Estimating global black carbon emissions using a top-down Kalman Filter approach. *Journal of Geophysical Research: Atmospheres*, *119*(1), 307-323.

Cohen, J. B., Prinn, R. G., & Wang, C. (2011). The impact of detailed urban-scale processing on the composition, distribution, and radiative forcing of anthropogenic aerosols. *Geophysical Research Letters*, *38*(10).

Collins, W. J., Fry, M. M., Yu, H., Fuglestvedt, J. S., Shindell, D. T., and West, J. J. (2013) Global and regional temperature-change potentials for near-term climate forcers, *Atmos. Chem. Phys.*, 13, 2471–2485.

Cox, L. (1999). Nitrogen oxides (NOx) why and how they are controlled. *Diane Publishing*.

Crutzen, P. J. (1970). The influence of nitrogen oxides on the atmospheric ozone content. *Quarterly Journal of the Royal Meteorological Society*, *96*(408), 320-325.

de Foy, B., Wilkins, J. L., Lu, Z., Streets, D. G., & Duncan, B. N. (2014). Model evaluation of methods for estimating surface emissions and chemical lifetimes from satellite data. *Atmospheric Environment*, *98*, 66-77.

Deng, W., Cohen, J. B., Wang, S., & Lin, C. (2021). Improving the understanding between climate variability and observed extremes of global NO_2 over the past 15 years. *Environmental Research Letters*, *16*(5), 054020.

Drysdale, W. S., Vaughan, A. R., Squires, F. A., Cliff, S. J., Metzger, S., Durden, D., ... & Lee, J. D. (2022). Eddy Covariance Measurements Highlight Sources of Nitrogen Oxide Emissions Missing from Inventories for Central London. *Atmospheric Chemistry and Physics Discussions*, 1-35.

Evangeliou, N., Thompson, R. L., Eckhardt, S., & Stohl, A. (2018). Top-down estimates of black carbon emissions at high latitudes using an atmospheric transport model and a Bayesian inversion framework, Atmos. Chem. Phys., 18, 15307–15327.

Geddes, J. A., & Murphy, J. G. (2014). Observations of reactive nitrogen oxide fluxes by eddy covariance above two midlatitude North American mixed hardwood forests. *Atmospheric Chemistry and Physics*, *14*(6), 2939-2957.

Haszpra, L., Hidy, D., Taligás, T., & Barcza, Z. (2018). First results of tall tower based nitrous oxide flux monitoring over an agricultural region in Central Europe. *Atmospheric Environment*, *176*, 240-251.

He, Q., Qin, K., Cohen, J. B., Loyola, D., Li, D., Shi, J., & Xue, Y. (2020). Spatially and temporally coherent reconstruction of tropospheric NO_2 over China combining OMI and GOME-2B measurements. *Environmental Research Letters*, *15*(12), 125011.

Henderson, B. H., Pinder, R. W., Crooks, J., Cohen, R. C., Carlton, A. G., Pye, H. O. T., & Vizuete, W. (2012). Combining Bayesian methods and aircraft observations to constrain the HO + NO_2 reaction rate. *Atmospheric Chemistry and Physics*, *12*(2), 653-667.

Holmes, C. D., Prather, M. J., Søvde, O. A., & Myhre, G. (2013) Future methane, hydroxyl, and their uncertainties: key climate and emission parameters for future predictions, *Atmos. Chem. Phys.*, 13, 285–302.

Hu, Y.; Zang, Z.; Chen, D.; Ma, X.; Liang, Y.; You, W.; Pan, X.; Wang, L.; Wang, D.; Zhang, Z. (2022) Optimization and Evaluation of SO2 Emissions Based on WRF-Chem and 3DVAR Data Assimilation. *Remote Sens.* 14, 220.

Jacob, D. J., Heikes, E. G., Fan, S. M., Logan, J. A., Mauzerall, D. L., Bradshaw, J. D., ... & Sachse, G. W. (1996). Origin of ozone and NOx in the tropical troposphere: A photochemical analysis of aircraft observations over the South Atlantic basin. *Journal of Geophysical Research: Atmospheres*, *101*(D19), 24235-24250.

Jin, X., Zhu, Q., & Cohen, R. C. (2021). Direct estimates of biomass burning NO_x emissions and lifetimes using daily observations from TROPOMI. *Atmospheric Chemistry and Physics*, *21*(20), 15569-15587.

Karl, T., Graus, M., Striednig, M., Lamprecht, C., Hammerle, A., Wohlfahrt, G., ... & Lee, J. (2017). Urban eddy covariance measurements reveal significant missing NOx emissions in Central Europe. *Scientific reports*, *7*(1), 1-9.

Karplus, V. J., Zhang, S., & Almond, D. (2018). Quantifying coal power plant responses to tighter SO_2 emissions standards in China. *Proceedings of the National Academy of Sciences*, *115*(27), 7004-7009.

Kong, H., Lin, J., Chen, L., Zhang, Y., Yan, Y., Liu, M., Ni, R., Liu, Z., and Weng, H. (2022). Considerable Unaccounted Local Sources of NOx Emissions in China Revealed from Satellite. *Environmental Science & Technology*, 2022 56 (11), 7131-7142.

Laughner, J., & Cohen, R. (2019). Direct observation of changing NO_x lifetime in North American cities. *Science*, *366*(6466), 723-727.

Lee, H. H., Bar-Or, R. Z., & Wang, C. (2017). Biomass burning aerosols and the low-visibility events in Southeast Asia. *Atmospheric Chemistry and Physics*, *17*(2), 965-980.

Lee, J. D., Helfter, C., Purvis, R. M., Beevers, S. D., Carslaw, D. C., Lewis, A. C., ... & Nemitz, E. G. (2015). Measurement of NOx fluxes from a tall tower in

central London, UK and comparison with emissions inventories. *Environmental science & technology*, *49*(2), 1025-1034.

Lei Z., Jacob, D., Mickley, L., Marais, E., Cohan, D., Yoshida, Y., Duncan, B., González, & Chance, K. (2014) Anthropogenic emissions of highly reactive volatile organic compounds in eastern Texas inferred from oversampling of satellite (OMI) measurements of HCHO columns. *Environ. Res. Lett.*, 9, 114004.

Li, L., Hoffmann, M. R., & Colussi, A. J. (2018). Role of nitrogen dioxide in the production of sulfate during Chinese haze-aerosol episodes. *Environmental science & technology*, *52*(5), 2686-2693.

Li, M., Zhang, Q., Kurokawa, J. I., Woo, J. H., He, K., Lu, Z., ... & Zheng, B. (2017). MIX: a mosaic Asian anthropogenic emission inventory under the international collaboration framework of the MICS-Asia and HTAP. *Atmospheric Chemistry and Physics*, *17*(2), 935-963.

Liang, X., Huang, T., Lin, S., Wang, J., Mo, J., Gao, H., ... & Ma, J. (2019). Chemical composition and source apportionment of PM_1 and $PM_{2.5}$ in a national coal chemical industrial base of the Golden Energy Triangle, Northwest China. *Science of the Total Environment*, *659*, 188-199.

Lin, C., Cohen, J. B., Wang, S., Lan, R., & Deng, W. (2020). A new perspective on the spatial, temporal, and vertical distribution of biomass burning: quantifying a significant increase in CO emissions. *Environmental Research Letters*, *15*(10), 104091.

Lin, J. T., Liu, Z., Zhang, Q., Liu, H., Mao, J., & Zhuang, G. (2012). Modeling uncertainties for tropospheric nitrogen dioxide columns affecting satellite-based inverse modeling of nitrogen oxides emissions. *Atmospheric Chemistry and Physics*, *12*(24), 12255-12275.

Ling, Z., Huang, T., Zhao, Y., Li, J., Zhang, X., Wang, J., ... & Ma, J. (2017). OMI-measured increasing SO_2 emissions due to energy industry expansion and relocation in northwestern China. *Atmospheric Chemistry and Physics*, *17*(14), 9115-9131.

Liu, M., Lin, J., Kong, H., Boersma, K. F., Eskes, H., Kanaya, Y., ... & Wang, J. (2020). A new TROPOMI product for tropospheric NO_2 columns over East Asia with explicit aerosol corrections. *Atmospheric Measurement Techniques*, *13*(8), 4247-4259.

Logan, J. A. (1983). Nitrogen oxides in the troposphere: Global and regional budgets. *Journal of Geophysical Research: Oceans*, *88*(C15), 10785-10807.

Lueue, C., Wenig, M., Wagner, T., Klimm, O., Platt, U., & Jähne, B. (2001). Quantitative analysis of NO_x emissions from Global Ozone Monitoring Experiment satellite image sequences. *Journal of Geophysical Research: Atmospheres*, *106*(D6), 5493-5505.

Lund, M. T., Aamaas, B., Stjern, C. W., Klimont, Z., Berntsen, T. K., &

Samset, B. H. (2020). A continued role of short-lived climate forcers under the Shared Socioeconomic Pathways. *Earth Syst. Dynam.*, 11, 977–993.

Martin, R. V., Jacob, D. J., Chance, K., Kurosu, T. P., Palmer, P. I., & Evans, M. J. (2003). Global inventory of nitrogen oxide emissions constrained by space-based observations of NO_2 columns. *Journal of Geophysical Research: Atmospheres*, *108*(D17).

Martin, R. V., Sioris, C. E., Chance, K., Ryerson, T. B., Bertram, T. H., Wooldridge, P. J., ... & Flocke, F. M. (2006). Evaluation of space-based constraints on global nitrogen oxide emissions with regional aircraft measurements over and downwind of eastern North America. *Journal of Geophysical Research: Atmospheres*, *111*(D15).

Mavroidis, I., & Chaloulakou, A. (2011). Long-term trends of primary and secondary NO_2 production in the Athens area. Variation of the NO_2/NO_x ratio. *Atmospheric environment*, *45*(38), 6872-6879.

Mijling, B., Van Der A, R. J., & Zhang, Q. (2013). Regional nitrogen oxides emission trends in East Asia observed from space. *Atmospheric Chemistry and Physics*, *13*(23), 12003-12012.

Monks, P. S., Archibald, A. T., Colette, A., Cooper, O., Coyle, M., Derwent, R., Fowler, D., Granier, C., Law, K. S., Mills, G. E., Stevenson, D. S., Tarasova, O., Thouret, V., von Schneidemesser, E., Sommariva, R., Wild, O., and Williams, M. L. (2015) Tropospheric ozone and its precursors from the urban to the global scale from air quality to short-lived climate forcer, *Atmos. Chem. Phys.*, 15, 8889–8973.

Napelenok, S. L., Pinder, R. W., Gilliland, A. B., & Martin, R. V. (2008). A method for evaluating spatially-resolved NO_x emissions using Kalman filter inversion, direct sensitivities, and space-based NO_2 observations. *Atmospheric Chemistry and Physics*, *8*(18), 5603-5614.

Olivier, J. G. J., Bouwman, A. F., Van der Maas, C. W. M., & Berdowski, J. J. M. (1994). Emission database for global atmospheric research (EDGAR). *Environmental Monitoring and Assessment*, 31(1), 93-106.

Platz, J., Nielsen, O. J., Wallington, T. J., Ball, J. C., Hurley, M. D., Straccia, A. M., ... & Sehested, J. (1998). Atmospheric chemistry of the phenoxy radical, C6H5O ($\bullet$): UV spectrum and kinetics of its reaction with NO, NO_2, and O_2. *The Journal of Physical Chemistry A*, *102*(41), 7964-7974.

Rogelj, J., Schaeffer, M., Meinshausen, M., Shindell, D., Hare, W., Klimont, Z., Velders, G., Amann, M., & Schellnhuber, H. (2014). Disentangling the effects of CO2 and short-lived climate forcer mitigation. *Proceedings of the National Academy of Sciences*, 111, 46, 16325-16330.

Rollins, A. W., Browne, E. C., Min, K. E., Pusede, S. E., Wooldridge, P. J., Gentner, D. R., ... & Cohen, R. C. (2012). Evidence for NOx control over nighttime SOA formation. *Science*, *337*(6099), 1210-1212.

Sand, M., Berntsen, T., von Salzen, K. et al. (2016) Response of Arctic temperature to changes in emissions of short-lived climate forcers. *Nature Clim Change*, 6, 286–289.

Seinfeld, J. H. (1989). Urban air pollution: state of the science. *Science*, *243*(4892), 745-752.

Shen, Y., Zhang, X., Brook, J. R., Huang, T., Zhao, Y., Gao, H., & Ma, J. (2016). Satellite remote sensing of air quality in the Energy Golden Triangle in Northwest China. *Environmental Science & Technology Letters*, *3*(7), 275-279.

Shindell, D. T. et al. Simultaneously mitigating near-term climate change and improving human health and food security. *Science*, 335, 183–189 (2012).

Stavrakou, T., Müller, J. F., Bauwens, M., De Smedt, I., Lerot, C., Van Roozendael, M., ... & Song, Y. (2016). Substantial underestimation of post-harvest burning emissions in the North China Plain revealed by multi-species space observations. *Scientific Reports*, *6*(1), 1-11.

Stavrakou, T., Müller, J. F., Boersma, K. F., De Smedt, I., & Van Der A, R. J. (2008). Assessing the distribution and growth rates of NO_x emission sources by inverting a 10-year record of NO_2 satellite columns. *Geophysical Research Letters*, *35*(10).

Stavrakou, T., Müller, J. F., Boersma, K. F., Van Der A, R. J., Kurokawa, J., Ohara, T., & Zhang, Q. (2013). Key chemical NO_x sink uncertainties and how they influence top-down emissions of nitrogen oxides. *Atmospheric Chemistry and Physics*, *13*(17), 9057-9082.

Streets, D. G., & Waldhoff, S. T. (2000). Present and future emissions of air pollutants in China: SO_2, NO_x, and CO. *Atmospheric Environment*, *34*(3), 363-374.

Tan, Z., Lu, K., Dong, H., Hu, M., Li, X., Liu, Y., ... & Zhang, Y. (2018). Explicit diagnosis of the local ozone production rate and the ozone-NOx-VOC sensitivities. *Science bulletin*, *63*(16), 1067-1076.

Tang, L., Xue, X., Qu, J., Mi, Z., Bo, X., Chang, X., ... & Dong, G. (2020). Air pollution emissions from Chinese power plants based on the continuous emission monitoring systems network. *Scientific Data*, *7*(1), 1-10.

Tong, Z., Li, Y., Lin, Q., Wang, H., Zhang, S., Wu, Y., & Zhang, K. M. (2022). Uncertainty investigation of plume-chasing method for measuring on-road NO_x emission factors of heavy-duty diesel vehicles. *Journal of Hazardous Materials*, *424*, 127372.

van Amstel, A., Olivier, J., & Janssen, L. (1999). Analysis of differences between national inventories and an Emissions Database for Global Atmospheric Research (EDGAR). *Environmental Science & Policy*, *2*(3), 275-293.

van der A, R. J., de Laat, A. T. J., Ding, J., & Eskes, H. J. (2020). Connecting the dots: NOx emissions along a West Siberian natural gas pipeline. *npj Climate*

and Atmospheric Science, *3*(1), 1-7.

van Der A, R. J., Eskes, H. J., Boersma, K. F., Van Noije, T. P. C., Van Roozendael, M., De Smedt, I., ... & Meijer, E. W. (2008). Trends, seasonal variability and dominant NOx source derived from a ten year record of NO2 measured from space. *Journal of Geophysical Research: Atmospheres*, *113*(D4).

Van Geffen, J., Boersma, K. F., Eskes, H., Sneep, M., Ter Linden, M., Zara, M., & Veefkind, J. P. (2020). S5P TROPOMI NO_2 slant column retrieval: method, stability, uncertainties and comparisons with OMI. *Atmospheric Measurement Techniques*, *13*(3), 1315-1335.

Vaughan, A. R., Lee, J. D., Misztal, P. K., Metzger, S., Shaw, M. D., Lewis, A. C., ... & Karl, T. G. (2016). Spatially resolved flux measurements of NO_x from London suggest significantly higher emissions than predicted by inventories. *Faraday discussions*, *189*, 455-472.

Veefkind, J. P., Aben, I., McMullan, K., Förster, H., De Vries, J., Otter, G., ... & Levelt, P. F. (2012). TROPOMI on the ESA Sentinel-5 Precursor: A GMES mission for global observations of the atmospheric composition for climate, air quality and ozone layer applications. *Remote sensing of environment*, *120*, 70-83.

Verhoelst, T., Compernolle, S., Pinardi, G., Lambert, J. C., Eskes, H. J., Eichmann, K. U., ... & Zehner, C. (2021). Ground-based validation of the Copernicus Sentinel-5p TROPOMI NO_2 measurements with the NDACC ZSL-DOAS, MAX-DOAS and Pandonia global networks. *Atmospheric Measurement Techniques*, *14*(1), 481-510.

Wang, S., Cohen, J. B., Deng, W., Qin, K., & Guo, J. (2021). Using a New Top-Down Constrained Emissions Inventory to Attribute the Previously Unknown Source of Extreme Aerosol Loadings Observed Annually in the Monsoon Asia Free Troposphere. *Earth's Future*, *9*(7), e2021EF002167.

Wang, S., Streets, D. G., Zhang, Q., He, K., Chen, D., Kang, S., ... & Wang, Y. (2010). Satellite detection and model verification of NO_x emissions from power plants in Northern China. *Environmental Research Letters*, *5*(4), 044007.

Wang, S. W., Zhang, Q., Streets, D. G., He, K. B., Martin, R. V., Lamsal, L. N., ... & Lu, Z. (2012). Growth in NOx emissions from power plants in China: bottom-up estimates and satellite observations. *Atmospheric Chemistry and Physics*, *12*(10), 4429-4447.

Zhang, X., & Schreifels, J. (2011). Continuous emission monitoring systems at power plants in China: Improving SO_2 emission measurement. *Energy Policy*, *39*(11), 7432-7438.

Zhao, C., & Wang, Y. (2009). Assimilated inversion of NO_x emissions over east Asia using OMI NO_2 column measurements. *Geophysical Research Letters*, *36*(6).

Zheng, Y. & Unger, N. (2021). Reducing planetary health risks through short-lived climate forcer mitigation. *GeoHealth*, 5, e2021GH000422

Zyrichidou, I., Koukouli, M. E., Balis, D., Markakis, K., Poupkou, A., Katragkou, E., ... & Van Roozendael, M. (2015). Identification of surface NO_x emission sources on a regional scale using OMI NO_2. *Atmospheric Environment*, *101*, 82-93.